nature communications

Article

https://doi.org/10.1038/s41467-025-60565-z

Echs1-mediated histone crotonylation facilitates zygotic genome activation and expression of repetitive elements in early mammalian embryos

Received: 22 October 2024

Accepted: 28 May 2025

Published online: 01 July 2025

Check for updates

Yong-feng Wang[1,6], Yu-ting Wan[1,6], Qian-rong Qi[2,6], Qing Tian[3], Xin-mei Liu[4], Qing-zhen Xie[2] ✉, Ying Yin[5] ✉ & Li-quan Zhou[1,4] ✉

Histone crotonylation, a conserved post-translational histone modification, plays a crucial role in transcriptional regulation. However, its function in early embryonic development remains largely unexplored. Here, we perform genome-wide mapping of histone crotonylation in mouse and human early embryos. Our analysis reveals that histone crotonylation is highly enriched at promoter regions and exhibits distinct dynamic patterns throughout embryogenesis. Notably, strong histone crotonylation signals are observed at the mouse 2-cell and human 4-to-8-cell stages, coinciding with zygotic genome activation. In mice, *Echs1* knockdown in oocytes, which suppresses histone crotonylation, results in developmental arrest at the 2-cell stage. Further investigation demonstrates that reduced histone crotonylation impairs transcriptional activity at zygotic genome activation genes, retrotransposon elements, and ribosomal DNA loci. Moreover, early embryos from aged female mice exhibit significantly diminished histone crotonylation, while supplementation with exogenous sodium crotonate enhances blastocyst formation. Collectively, our findings establish histone crotonylation as a key regulatory mechanism in early mammalian embryogenesis by facilitating transcriptional activation of zygotic genome activation genes and repetitive elements.

The transition from fertilization to early embryonic development is a highly intricate process, tightly regulated across multiple stages in mammals. A critical event in preimplantation development is zygotic genome activation (ZGA), which initiates at the 2-cell stage in mice and the 4-to-8-cell stage in humans, marking the onset of autonomous gene expression[1]. In mice, the previously inactive zygotic genome undergoes two distinct transcriptional waves after fertilization: minor ZGA at the early 2-cell stage and major ZGA at the late 2-cell stage[2]. Histone modifications are pivotal in regulating ZGA by influencing chromatin opening, transcriptional activity, and early developmental programs[3–5]. Disruptions to these modifications impair transcription, resulting in abnormal embryonic development[6,7].

During the ZGA period in cleavage-stage embryos, histone modifications are tightly coordinated with specific developmental stages and genomic regions, ensuring precise transcription required for normal development. For example, as ZGA occurs, levels of H3K4me3

[1]Institute of Reproductive Health, Tongji Medical College, Huazhong University of Science and Technology, Wuhan, Hubei, China. [2]Center for Reproductive Medicine, Renmin Hospital of Wuhan University, Wuhan, Hubei, China. [3]Department of Gynecology and Obstetrics, Zhongnan Hospital of Wuhan University, Wuhan, Hubei, China. [4]Shanghai Key Laboratory of Reproduction and Development, Shanghai, China. [5]Department of Physiology, School of Basic Medicine, Tongji Medical College, Huazhong University of Science and Technology, Wuhan, Hubei, China. [6]These authors contributed equally: Yong-feng Wang, Yu-ting Wan, Qian-rong Qi. ✉e-mail: rm001138@whu.edu.cn; yinying@hust.edu.cn; zhouliquan@hust.edu.cn

and H3K27ac increase significantly, promoting the activation of embryonic genes and initiating the transcriptional program[8,9]. In contrast, modifications such as H3K9me3 and H3K27me3 are linked to gene repression and heterochromatin formation, maintaining the silencing of specific genomic regions. Among these regulatory mechanisms[10,11], histone methylation and acetylation have been extensively studied and are well-characterized during the cleavage stages of embryonic development, providing insight into the transcriptional regulatory networks involved.

Histone lysine crotonylation (Kcr) is a conserved histone modification that plays a critical role in transcriptional regulation[12]. Crotonyl-CoA, the primary substrate for histone Kcr, is produced through multiple metabolic pathways[13]. The conversion of crotonate into crotonyl-CoA is catalyzed by Acyl-CoA synthetase short-chain family member 2 (ACSS2)[14]. Additionally, the short-chain enoyl−coenzyme A (CoA) hydratase encoded by ECHS1 regulates histone Kcr levels[15,16]. ECHS1 has been implicated in promoting endoderm differentiation of embryonic stem cells, maintaining cardiomyocyte maturation and homeostasis, and constraining tumor progression[13,15–17]. Furthermore, Chromodomain Y-like protein (CDYL) functions as a crotonyl-CoA hydratase, reducing crotonyl-CoA availability and thereby negatively regulating histone Kcr[18]. Recent studies have identified enzymes responsible for both the addition and the removal of histone Kcr[19–21]. For example, P300-mediated histone Kcr enhances gene transcription more effectively than P300-mediated histone lysine acetylation (Kac)[14]. Histone Kcr marks active chromatin regions, particularly at enhancers and promoters, highlighting its role in transcriptional activition[14]. This modification is involved in a range of biological processes, including stem cell differentiation[13], cancer progression[15], hypertrophic cardiomyopathy[16] spermatogenesis[22], and oocyte maturation[23]. However, its function in initiating transcription during early embryonic development remains poorly understood.

In this study, we demonstrate that *Echs1* regulates histone Kcr in cleavage-stage mouse embryos and that sufficient histone Kcr at embryonic gene promoters is essential for embryonic progression beyond the 2-cell stage. Mechanistically, inadequate histone Kcr impairs ZGA, disrupts retrotransposon regulation, and perturbs rRNA synthesis. A positive correlation between histone Kcr and transcription was also observed in human cleavage embryos, suggesting a conserved role in human embryonic transcriptional regulation, including ZGA. Together, our findings establish histone Kcr as a key regulator of ZGA and repetitive element expression in early mammalian development.

Results

Histone Kcr is positively correlated with global transcriptional activity in early mouse embryos

To explore the role of histone acylation in regulating transcription during early mouse embryonic development, we conducted a comparative exposure experiment by supplementing the embryo culture medium with epigenetic metabolites—key substrates for histone modifications. We tested four metabolites: sodium crotonate, sodium acetate, sodium lactate, and sodium β- hydroxybutyrate[24–26]. Mouse zygotes were exposed to these metabolites, and early 2-cell embryos were collected for immunofluorescence (IF) staining and mRNA quantification. The results revealed a moderate increase in the corresponding histone modifications (Fig. 1A) and an upregulation of representative ZGA genes (Fig. 1B, C). Notably, sodium crotonate induced the most significant increase in ZGA gene expression compared to the other metabolites. Furthermore, IF staining of 5′-ethyluracil (EU) and histone Kcr in 2-cell embryos demonstrated a positive correlation between de novo transcriptional activity and nuclear histone Kcr levels (Fig. 1D).

Next, we examined the dynamic distribution of histone Kcr across the mouse genome during early embryonic development. By staining two histone Kcr modifications, H3K9cr and H3K4cr, at various developmental stages, we observed a progressive increase in histone Kcr levels from the oocyte to the 2-cell stage, followed by a sharp decline at the 4-cell stage, and a subsequent rise after the 8-cell stage (Supplementary Fig. 1A, B). We also analyzed H3K27ac dynamics across different developmental stages in oocytes and preimplantation embryos, observing a marked decline of H3K27ac at the 4-cell stage (Supplementary Fig. 1C). This finding aligns with our previous research, which demonstrated a significant reduction in actively transcribed genes at the 4-cell stage, labeled by S2-phosphorylated RNA polymerase II (Pol II) peaks (Supplementary Fig. 1D)[27]. The decrease in chromatin opening and transcription activity at this stage may stem from elevated DNA replication stress and genome instability, which are uniquely pronounced in mouse 4-cell embryos[28].

To further investigate histone Kcr dynamics, we performed CUT&Tag profiling of H3K9cr in mouse germinal vesicle (GV) oocytes and early embryos spanning the 2-cell to morula stages (Fig. 1E). Correlation analysis revealed that H3K9cr enrichment at the 2-cell stage closely resembled that of the GV stage, whereas H3K9cr levels at the 4-cell stage deviated significantly from other stages (Fig. 1F). Hierarchical clustering analysis confirmed the reproducibility of our sequencing data (Supplementary Fig. 1E). Notably, genomic feature analysis of H3K9cr peaks indicated a substantial enrichment of histone Kcr signals at promoter regions in early 2-cell embryos (Fig. 1G), highlighting its potential role in regulating ZGA. Additionally, we examined H3K4cr and Pol II occupancy in early 2-cell embryos (Supplementary Fig. 1F, G) and found that H3K9cr and H3K4cr exhibited highly similar distribution patterns. Both modifications were enriched at Pol II peaks, reinforcing the strong correlation between histone Kcr and transcriptional activity in early embryos.

To classify genes based on H3K9cr dynamics from oocytes to early embryos (Supplementary Fig. 1H), we performed k-means clustering[29] using H3K9cr intensities at gene promoters across developmental stages. This analysis identified 40 distinct clusters (Supplementary Fig. 2A). We categorized these clusters into three major groups based on their H3K9cr patterns (Fig. 1H). The ‘MAT-CRO’ group included genes with high H3K9cr levels in GV oocytes, which rapidly declined during cleavage embryogenesis. This group contained typical maternal genes, such as *Nobox*. Gene ontology (GO) analysis revealed enrichment in biological processes related to intracellular signal transduction and cell adhesion. The ‘E2C-CRO’ and ‘L2C-CRO’ groups consisted of genes with transient H3K9cr enrichment at the early and late 2-cell stages, respectively. These groups included key ZGA genes, such as *Zfp352* and members of the *Zscan4* family. GO analysis of these genes highlighted their involvement in gene expression-related processes.

To further investigate the functional relationship between histone Kcr and transcriptional activity during early embryonic development, we treated early mouse embryos with 5,6-dichloro-1-β-D-ribofuranosylbenzimidazole (DRB), a reversible inhibitor of Pol II elongation[30]. DRB treatment arrested embryos at the 2-cell stage, significantly reduced histone Kcr levels (Supplementary Fig. 3A, B), and suppressed ZGA activity, as confirmed by qRT-PCR in 2-cell embryos (Supplementary Fig. 3C). Consistently, we observed that Pol II and H3K9cr signals accumulated at gene promoter regions when transcription elongation was inhibited (Fig. 1I, J). Additionally, we examined early 2-cell embryos exposed to sodium crotonate and found that Pol II signals increased at both gene promoter and gene body regions (Fig. 1K), further supporting the role of histone Kcr in promoting transcriptional activity during early embryogenesis.

Together, our findings reveal a strong positive correlation between histone Kcr and transcriptional activity in early mouse embryos, suggesting a crucial role for histone Kcr in regulating ZGA genes and early embryonic development.

https://doi.org/10.1038/s41467-025-60565-z

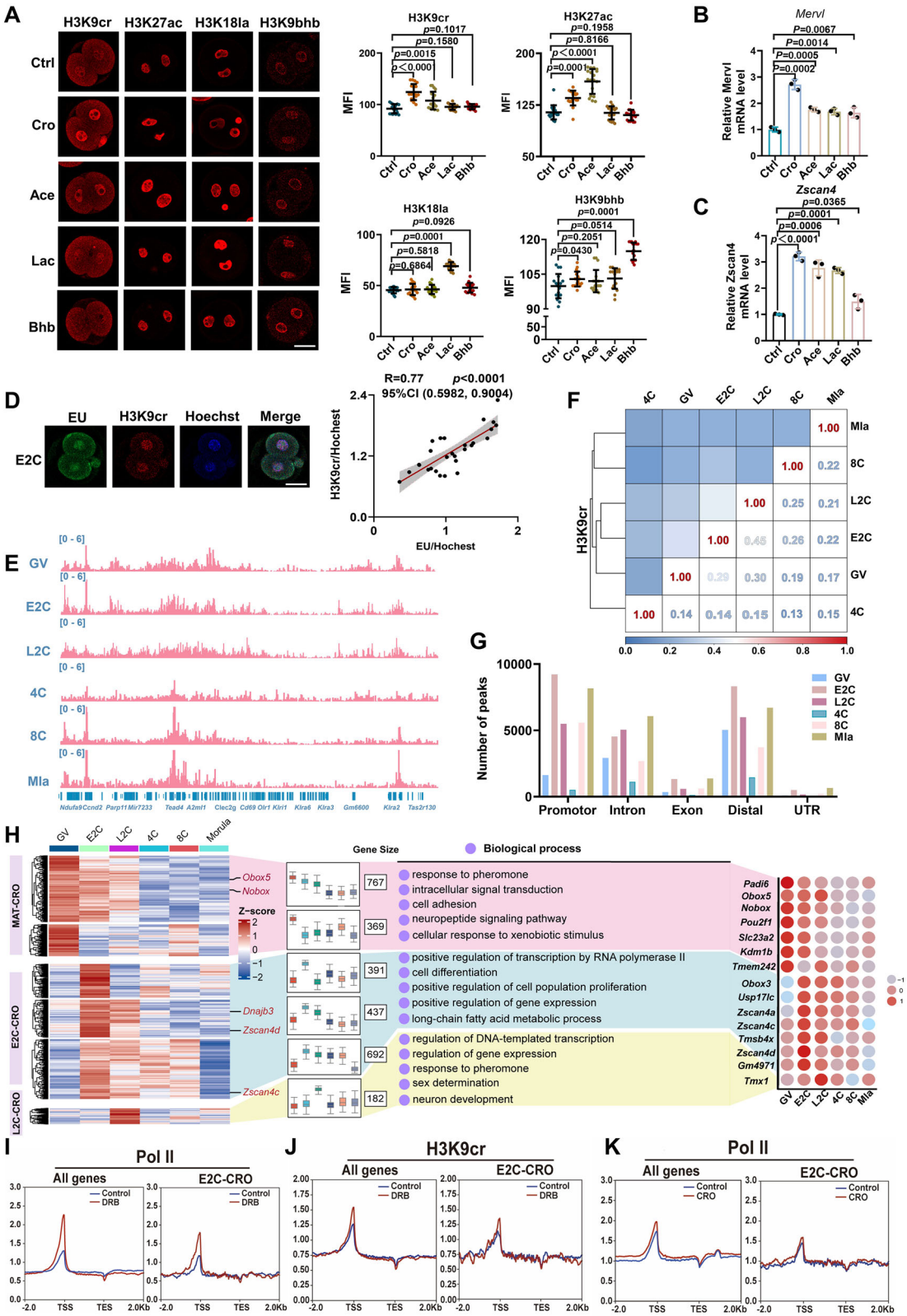

Suppression of histone Kcr by *Echs1* deficiency in early mouse embryos causes 2-cell arrest

Crotonyl-CoA, an endogenous intermediate metabolite, plays a central role in fatty acid oxidation and tryptophan/lysine degradation and serves as a substrate for histone Kcr modification[13,14,31]. To investigate the function of histone Kcr in early embryonic development, we targeted key enzymes involved in crotonyl-CoA production (Fig. 2A). We achieved this by injecting siRNA into oocytes, which were then matured, fertilized, and cultured for further embryonic development (Fig. 2B).

Initially, we focused on *Acss2*, a well-characterized enzyme responsible for crotonyl-CoA production. However, inhibition of ACSS2 via exogenous inhibitors did not affect histone Kcr levels in early embryos (Supplementary Fig. 4A) or alter ZGA gene expression

Fig. 1 | Histone Kcr is critical for early embryonic development in mice. **A** Immunofluorescence staining and mean fluorescence intensities (MFI) of H3K9cr, H3K27ac, H3K18la and H3K9bhb in early 2-cell embryos treated by sodium crotonate (Cro), sodium acetate (Ace), sodium lactate (Lac), or β-hydroxybutyric acid (Bhb) from early zygote stage ($n = 18$). Scale bars: 20 μm. **B, C** qRT-PCR showed the expression of *Mervl* (**B**) and *Zscan4* (**C**) in early 2-cell embryos treated with epigenetic metabolites ($n = 30$). **D** Immunofluorescence co-staining and Pearson correlation analysis of EU and H3K9cr signals in early 2-cell embryos, the experiment was conducted with three independent biological replicates, ($n = 28$). CI: confidence interval. Scale bars: 20 μm. **E** Genomic view of H3K9cr occupancy in GV oocyte and preimplantation embryo by IGV browser. **F** Spearman correlation analysis of genome-wide H3K9cr read counts at various developmental stages. **G** The number of H3K9cr peaks at different genomic regions including promoter, intron, exon, UTR and distal regions across various developmental stages. **H** Heatmap shows hierarchical clustering of H3K9cr intensity at promoter regions across developmental stages, with row-normalized values color-coded. Representative genes in each cluster were marked. Three gene clusters with similar H3K9cr change patterns were named 'MAT-CRO', 'E2C-CRO', and 'L2C-CRO'. Boxplots display H3K9cr intensity trends for each cluster during embryonic development, the boxplot composition (centre line: median; box limits: quartile 1 and quartile 3, and whiskers showing the maximum and minimum values). On the right are GO analysis results for the three gene classes and a dot plot of H3K9cr intensity normalized count changes for typical maternal and ZGA genes. **I–K** Metaplots display the average Pol II (**I**) or H3K9cr (**J**) enrichment signals at TSS and TES of all genes or 'E2C-CRO' group genes in early 2-cell embryos treated with DRB. In early 2-cell embryos treated with sodium crotonate (**K**), metaplots showed higher enrichment signals of Pol II at TSS regions of all genes or 'E2C-CRO' group genes. In (**A**), (**B**) and (**C**), data were presented as Mean ± SD of three independent replicates, and statistical evaluation was performed by two-tailed unpaired Student's *t*-test. Source data are provided as a Source Data file.

(Supplementary Fig. 4B). Furthermore, *Acss2* knockdown had no detectable impact on H3K9cr modification levels (Supplementary Fig. 4C, D). These results suggest that ACSS2 does not serve as a key regulator of histone Kcr in early mouse embryos.

Next, we investigated the expression of regulators involved in histone Kcr modification using a publicly available RNA-seq dataset (Fig. 2C, Supplementary Fig. 4E). We noticed that both *Acox3* and *Echs1* genes are enriched in mouse oocytes and 2-cell embryos, suggesting their potential roles in promoting histone Kcr. Initially, we knocked down *Acox3* (Supplementary Fig. 5A) and monitored embryonic development. However, we observed no developmental abnormalities, and histone Kcr levels remained unchanged following *Acox3* knockdown (Supplementary Fig. 5B–D). Interestingly, we found that *Echs1* exhibited expression patterns that mirrored the dynamics of histone Kcr in early embryos (Fig. 2C and Supplementary Fig. 1A, B). IF staining further revealed a similar expression pattern for ECHS1 protein (Supplementary Fig. 6A). Based on these observations, we proceeded with *Echs1* knockdown in oocytes to assess its impact on embryonic development. We designed two siRNA sequences targeting *Echs1*, both of which efficiently reduced ECHS1 protein expression in oocytes. The combined injection of both siRNAs resulted in higher knockdown efficiency compared to individual siRNA injections (Supplementary Fig. 6B). Therefore, we used the combined injection of both siRNAs in all subsequent experiments. Notably, *Echs1* knockdown led to a reduction in histone Kcr levels (Supplementary Fig. 6C, D).

To obtain early 2-cell embryos with *Echs1* knockdown, we matured *Echs1*-deficient oocytes, fertilized them, and cultured the embryos. IF and immunoblotting confirmed the successful knockdown of *Echs1* in the 2-cell embryos (Fig. 2D, E). Additionally, histone Kcr levels were reduced in the 2-cell stage embryos (Fig. 2F, G). Further analysis of histone modifications revealed that *Echs1* knockdown led to a decrease in H3K9ac levels and an increase in H3K9me3 levels (Supplementary Fig. 6E–G), suggesting that the mouse genome was less accessible when histone Kcr was reduced. Moreover, *Echs1* knockdown resulted in embryo arrest at the 2-cell stage, whereas control embryos progressed to the blastocyst stage (Fig. 2H). To investigate the impact of histone Kcr on early embryonic development, we conducted a 5-ethynyl-2′-deoxyuridine (EdU) incorporation assay. This revealed that cell proliferation in 2-cell embryos was impaired upon *Echs1* knockdown (Fig. 2I). Additionally, we performed a 5-EU incorporation assay to assess nascent transcriptional activity. This assay showed decreased transcription activity in 2-cell embryos with *Echs1* knockdown (Fig. 2J).

In summary, our findings indicate that *Echs1*-mediated histone Kcr is crucial for the proper execution of the embryonic developmental program, particularly for progression beyond the 2-cell stage in mice.

Echs1-mediated histone Kcr promotes transcription activity in early mouse 2-cell embryos

To investigate the molecular mechanisms driving developmental defects in *Echs1*-deficient early embryos, we performed RNA sequencing (RNA-seq) on control and *Echs1* knockdown 2-cell embryos. Clustering analysis revealed strong correlation among biological replicates (Supplementary Fig. 7A). A total of 2,677 genes were found to be dysregulated following *Echs1* knockdown, with 1,391 genes upregulated and 1,286 genes downregulated (Fig. 3A). Among the upregulated genes were several key maternal factors, including ZP3, *Padi6*, and *Zar1*, while downregulated genes included typical ZGA genes, such as *Zscan4a*, *Zfp352*, and *Usp17lb*. To better understand how *Echs1* affects the regulation of maternal RNA and minor ZGA gene sets[32], we analyzed these categories specifically. As anticipated, *Echs1* knockdown led to a global increase in the expression of maternal RNA genes and a decrease in the expression of minor ZGA genes (Fig. 3B–E). Additionally, we observed a significant downregulation of several mitochondrial-related genes (Fig. 3D). The analysis of the top 25 upregulated genes and the top 25 downregulated genes showed that the most upregulated genes were enriched at the MII phase, while the most downregulated genes were enriched at the early 2-cell stage (Supplementary Fig. 7B). This analysis further supports the notion that *Echs1* deficiency disrupts both maternal transcript degradation and embryonic gene activation. Genes exhibiting elevated expression in the early 2-cell embryos were predominantly associated with mitochondrial functions, including "mitochondrial ATP synthesis," "mitochondrial respiration," and "mitochondrial translation" (Supplementary Fig. 7C). In contrast, genes with lower expression were enriched in GO categories related to "positive regulation of gene expression" and "regulation of transcription by RNA polymerase II" (Supplementary Fig. 7D). Quantitative PCR (qRT-PCR) analysis confirmed the upregulation of maternal genes (Fig. 3F) and downregulation of minor ZGA genes (Fig. 3G), consistent with the RNA-seq data. Furthermore, IF staining revealed a reduction in ZSCAN4 and MERVL protein levels in *Echs1* knockdown 2-cell embryos (Supplementary Fig. 7E, F). These findings suggest that inhibition of *Echs1*-mediated histone Kcr disrupts normal transcriptional program during early 2-cell embryonic development.

To further investigate how histone Kcr regulates minor ZGA in early development, we performed CUT&Tag to examine the genome-wide distribution of H3K9cr and Pol II in control and *Echs1* knockdown early 2-cell embryos. Gene promoter regions were defined as -2 kb to +2 kb relative to the transcription start site (TSS), and gene body regions were defined as the +2 kb downstream of the TSS to the transcription end site (TES) (Supplementary Fig. 7G). In control 2-cell embryos, Pol II intensity at the TSS was positively correlated with both H3K9cr (Fig. 3H) and H3K4cr (Supplementary Fig. 7H) intensities. This positive correlation was also observed in the gene body regions

https://doi.org/10.1038/s41467-025-60565-z

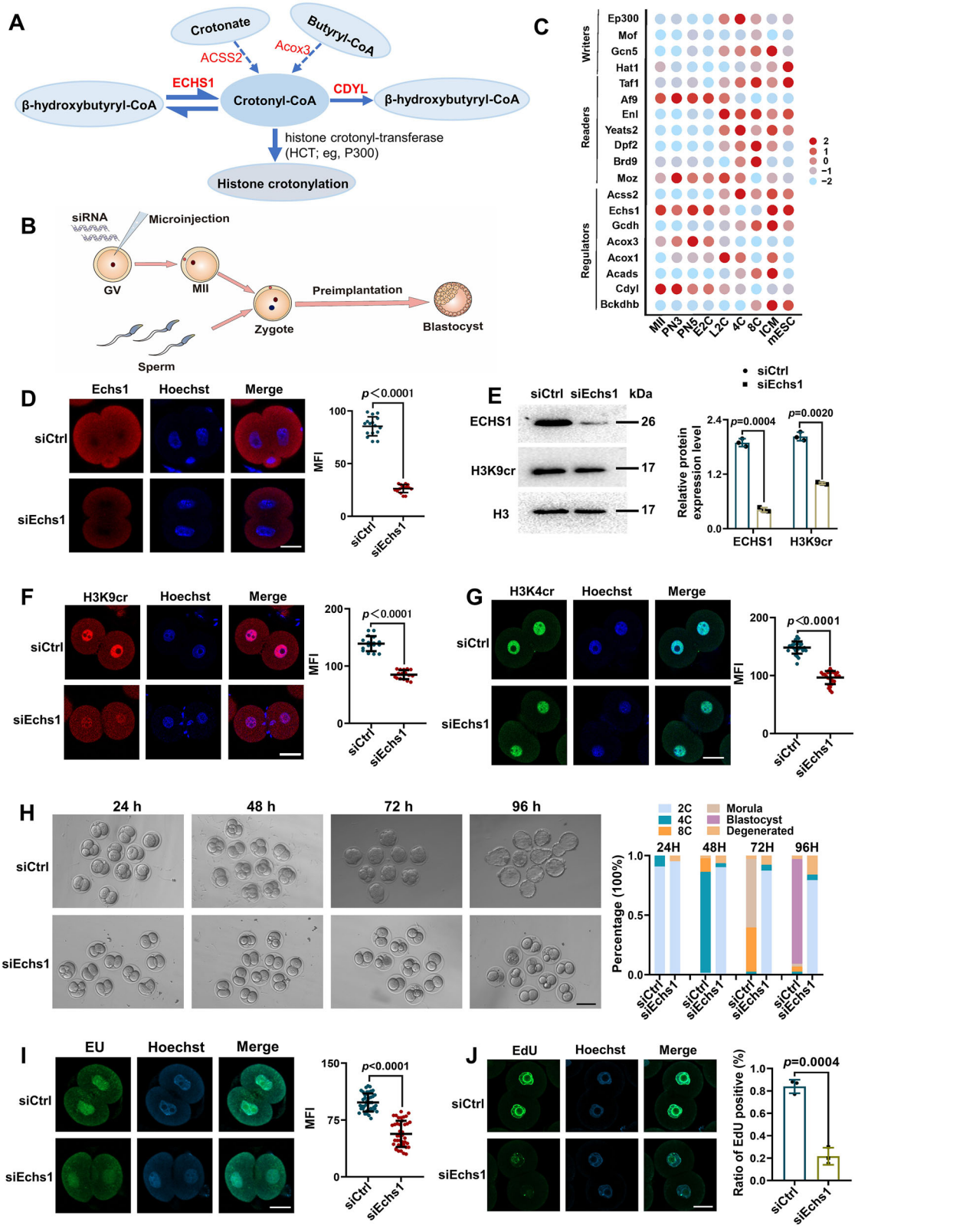

(Supplementary Fig. 7I, J). Additionally, a positive correlation between H3K9cr and H3K4cr intensities was found at both the TSS and gene body regions (Supplementary Fig. 7K, L). Notably, H3K9cr intensity showed a positive correlation with H3K9ac intensity (Supplementary Fig. 7M) and CpG density (Supplementary Fig. 7N) at the TSS. These results suggest that histone Kcr is closely linked to transcriptional activation in early embryos.

Echs1 knockdown embryos exhibited a significant reduction in Pol II intensity across all genic loci, and a similar pattern was observed when examining gene loci in the 'E2C-CRO' group (Fig. 3I). Furthermore, we observed a strong association between H3K9cr and 'minor ZGA' gene loci, rather than with 'maternal RNA' gene loci, during the early 2-cell stage (Fig. 3J). This suggests that histone Kcr directly influences transcriptional activation. In line with this, Pol II binding was

Fig. 2 | *Echs1* is the key regulator of histone Kcr in early mouse embryos. **A** Model diagram of key factors controlling histone crotonylation modification. Crotonyl-CoA and β-hydroxybutyryl-CoA can be interconverted by *Echs1*. In addition, crotonyl-CoA can be generated from crotonic acid catalyzed by *Acss2* or from Butyryl-CoA catalyzed by *Acox3*, and ultimately converted unidirectionally to β-hydroxybutyryl-CoA catalyzed by *Cdyl*. **B** Experimental design schematic for *Echs1* knockdown in oocytes, IVM, IVF, and preimplantation development of mouse embryos. Generally, siRNA was injected into GV oocytes for IVM, then MII oocytes were obtained for IVF, the zygotic and preimplantation embryos were obtained through culturing in KSOM medium. **C** Dotplot indicated expression changes of known histone Kcr writers, readers, and regulators in mouse oocytes and preimplantation embryos (log_2FPKM). The transcriptome data was derived from GSE165782. **D** Immunofluorescence staining and MFI of ECHS1 protein in early 2-cell embryos of *siCtrl* (control siRNA was injected) and *siEchs1* (siRNA against *Echs1* was injected) groups ($n = 16$). Scale bar: 20 μm. **E** Examination and quantification analysis of ECHS1, H3K9cr, and total histone H3 protein levels in *siCtrl* and *siEchs1* early 2-cell embryos by immunoblotting. The blots were derived from the same experiment and processed in parallel. Total histone H3 level was set as an internal reference ($n = 300$). **F, G** Immunofluorescence staining and MFI of H3K9cr (**F**) ($n = 16$) and H3K4cr (**G**) ($n = 27$) in *siCtrl* and *siEchs1* embryos. Scale bar: 20 μm. **H** Representative developmental progression images of early embryos. Different stage embryo percentages were shown to average on the right ($n = 3$ independent replicates). Scale bar: 100 mm. **I, J** Confocal images showed newly synthesized DNA by EU staining (**I**) ($n = 40$) and newly synthesized RNA by EdU staining (**J**) in *siCtrl* and *siEchs1* embryos ($n = 3$ independent replicates), scale bar: 20 μm, MFI and the percentages of positive EdU embryos was shown on the right of each image. In (**D**), (**E**), (**F**), (**G**), (**I**) and (**J**), data were presented as Mean ± SD of three independent replicates and statistical evaluation was performed by two-tailed unpaired Student's *t*-test. Source data are provided as a Source Data file.

stronger at 'minor ZGA' gene loci than at 'maternal RNA' loci during the early 2-cell stage, and Pol II intensity at 'minor ZGA' loci significantly decreased upon *Echs1* knockdown (Fig. 3K).

Mammalian genomes exhibit tissue-specific DNA methylation patterns, which can interact with other epigenetic modifications to suppress gene expression, particularly at the promoter regions[33,34]. Given that a significant proportion of histone Kcr peaks localized to the promoter regions in early embryos (Fig. 1G), it is plausible that there is crosstalk between histone Kcr and DNA methylation which may modulate gene expression in conjunction with histone Kcr. To explore this, we assessed DNA methylation changes in mouse genome of early 2-cell embryos with *Echs1* knockdown. Our analysis revealed a significant alteration in DNA methylation, with 12,752 genomic regions becoming hypermethylated and 2,205 regions exhibiting hypomethylation (Fig. 3L). Additionally, histone Kcr intensity negatively correlated with DNA methylation at gene promoter regions in early 2-cell embryos (Fig. 3M). *Echs1* knockdown led to a global increase in DNA methylation across the mouse genome (Fig. 3N), particularly at promoter regions (Fig. 3O). Further analysis revealed that methylation levels were elevated not only in promoter regions but also at 5' UTR, intron, exon, 3' UTR, and intergenic regions in *Echs1* knockdown early 2-cell embryos (Supplementary Fig. 8A–E). These findings suggest that *Echs1*-mediated histone Kcr counteracts DNA methylation, though the underlying mechanism remains to be fully understood.

RNA-seq analysis revealed the dysregulation of mitochondrial-related genes in *Echs1*-knockdown embryos, implying potential dysfunction of subcellular organelles, including mitochondria. As expected, we observed several mitochondrial abnormalities: mis-localization of mitochondria (Fig. 3P), elevated ROS levels (Fig. 3Q), disrupted mitochondrial membrane potential (Fig. 3R), reduced ATP levels (Fig. 3S), and decreased mitochondrial DNA (mtDNA) copy number (Fig. 3T). However, *Echs1* knockdown did not affect the localization of the Golgi apparatus or the endoplasmic reticulum (ER) (Supplementary Fig. 8F, G).

In summary, our results demonstrate that *Echs1*-mediated histone Kcr is associated with minor ZGA gene loci, playing a crucial role in gene activation during early 2-cell embryo development in mice.

Echs1-mediated histone Kcr facilitates expression of genes and repetitive elements in mouse late 2-cell embryos

We next examined whether histone Kcr reduction, caused by *Echs1* knockdown, affected major ZGA. To address this, we performed RNA-seq analysis on control and *Echs1*-knockdown late 2-cell embryos. Clustering analysis of biological replicates showed strong correlation among the RNA-seq samples (Supplementary Fig. 9A). A total of 4,564 upregulated genes and 4,800 downregulated genes were identified in the *Echs1*-knockdown late 2-cell embryos (Fig. 4A). Consistent with the early 2-cell stage, *Echs1* knockdown in late 2-cell embryos led to an increase in the expression of maternal RNA genes and a decrease in minor ZGA gene expression (Fig. 4B, C). Moreover, we observed a significant reduction in the expression of major ZGA genes (Fig. 4D)[32]. GO enrichment analysis of differentially expressed genes revealed a similar pattern to that observed in the early 2-cell embryos, with upregulated genes associated with mitochondrial metabolism and downregulated genes linked to transcriptional regulation (Supplementary Fig. 9B, C). Specifically, typical maternal factors such as *Padi6* and *Zp3* were upregulated, while minor ZGA genes, including *Zscan4* family members, and major ZGA genes, such as *Cdk9* and *Tomm20*, were downregulated in *Echs1*-knockdown late 2-cell embryos (Fig. 4E, F). When mouse embryos were treated with sodium crotonate from early to late 2-cell stage, we noticed upregulation of major ZGA, supporting that histone crotonylation activates major ZGA (Supplementary Fig. 9D).

Correlation analysis revealed that H3K9cr intensity at the TSS in late 2-cell embryos was positively correlated with Pol II enrichment (Fig. 4G) and mRNA levels of major ZGA genes, as determined by RNA-seq (Fig. 4H). Additionally, the enrichment of H3K9cr at TSS regions correlated with its presence at gene body regions (Fig. 4I). These results suggest that histone Kcr plays a positive role in the expression of major ZGA genes.

Our analysis revealed inhibited DNA replication in 2-cell stage embryos following *Echs1* knockdown (Fig. 2J). While cell cycle dysregulation typically leads to embryonic arrest[35], it does not necessarily block ZGA activity[36]. To further investigate, we treated early 2-cell embryos with aphidicolin (APH), a drug that inhibits DNA replication by blocking DNA polymerase activity. We then collected late 2-cell embryos to assess the impact of DNA replication inhibition on ZGA gene expression. EdU staining confirmed that DNA replication was inhibited (Fig. 4J). We found that despite the inhibition of DNA replication, the activation of both minor and major ZGA genes was almost unaffected (Fig. 4K, L). These findings suggest that impaired DNA replication is not the cause of failed major ZGA in *Echs1*-knockdown 2-cell embryos.

Previous studies have shown that retrotransposons, such as long interspersed nuclear elements (LINEs), short interspersed nuclear elements (SINEs), and long terminal repeats (LTRs), exhibit stage-specific expression and contribute to the regulation of early embryonic development[37]. Histone modifications influence the expression of retrotransposons by altering chromatin structure, thereby maintaining genome stability and controlling gene expression[38]. Our transcriptome analysis revealed that retrotransposons, including LINEs, SINEs, and LTRs, exhibited only mild expression changes at the early 2-cell stage following *Echs1* knockdown (Supplementary Fig. 10A–D). However, *Echs1* deficiency severely impaired the expression of retrotransposons at the late 2-cell stage (Fig. 4M), particularly the SINE/B1 family, which was notably downregulated in *Echs1* knockdown late 2-cell embryos. Further analysis revealed that the SINE family members showed the

https://doi.org/10.1038/s41467-025-60565-z

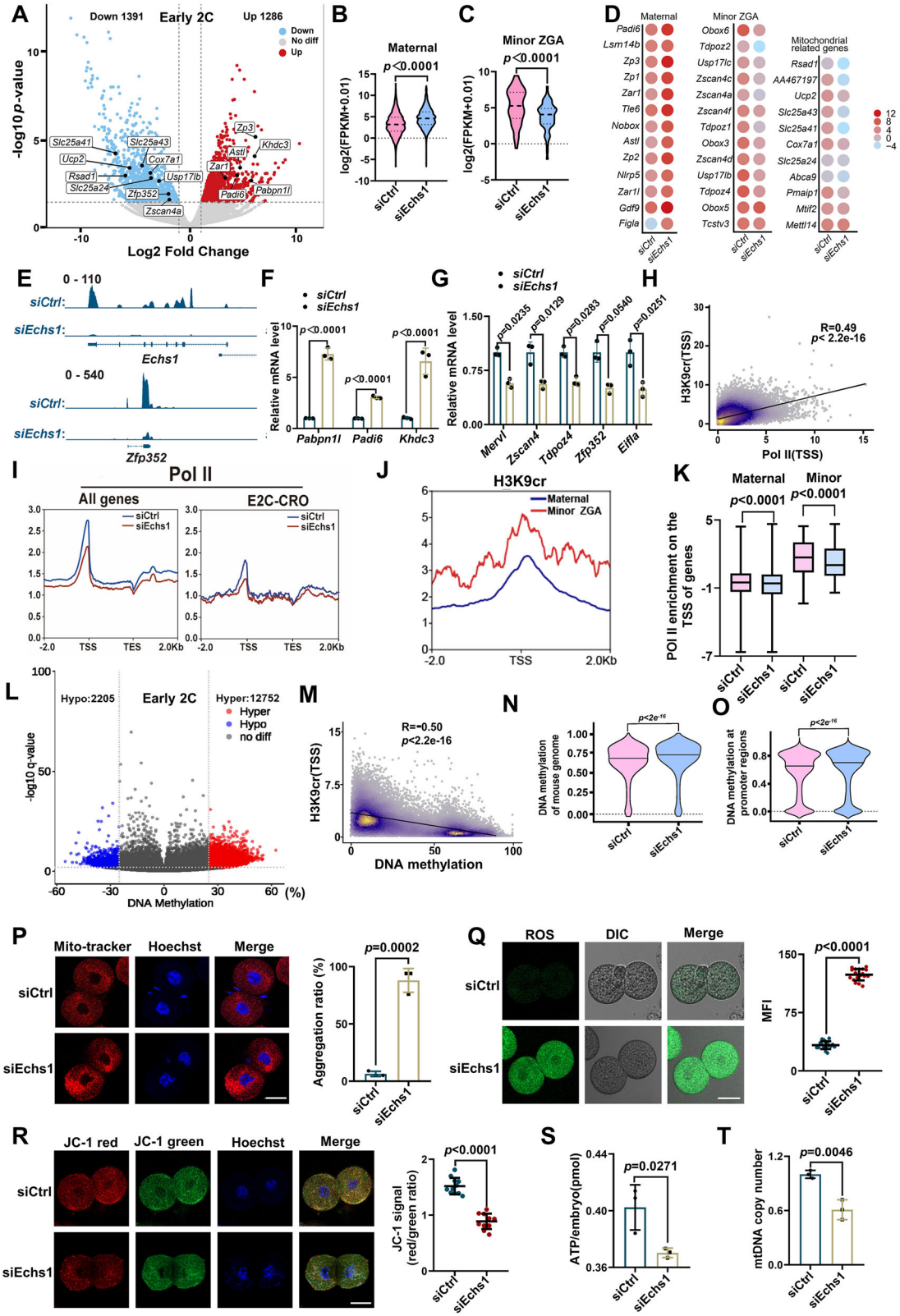

most significant reduction in expression, although LTRs and LINEs also exhibited decreased expression levels (Fig. 4N and Supplementary Fig. 10E–G). Genome-wide occupancy analysis demonstrated that regions enriched in H3K9cr at the loci of LINEs, SINEs, and LTRs, particularly those of SINE family members, were consistently associated with stronger Pol II binding (Supplementary Fig. 10H). When we filtered retrotransposons based on an H3K9cr enrichment index greater than 1, we primarily identified SINE/B1 elements, and these elements exhibited a positive correlation between higher H3K9cr enrichment and increased Pol II occupancy (Supplementary Fig. 10I). In contrast, LTR and LINE family members with an enrichment index greater than 1 showed divergent patterns between H3K9cr enrichment and Pol II binding (Supplementary Fig. 10J, K). Notably, the expression of many retrotransposons, particularly those with high H3K9cr intensities, was downregulated in the *Echs1* knockdown group (Supplementary Fig. 10J, K).

Fig. 3 | *Echs1*-mediated histone Kcr is critical for minor ZGA in early 2-cell embryos in mice. A Volcano of transcript changes in *siEchs1* versus *siCtrl* early 2-cell embryos (*p*-value were calculated using DESeq2). Representative mitochondria-related genes, 'maternal RNA' and 'minor ZGA' genes were indicated. **B, C** Violin plots demonstrated transcriptional differences (Mean ± SD) of 'maternal RNA' (**B**) and 'minor ZGA' (**C**) genes (GSE169632) between early 2-cell embryos. **D** Dotplots indicated different expressed genes of early 2-cell embryos. **E** Genome browser view of RNA- seq results of early 2-cell embryos by IGV. **F, G** qRT-PCR results of 'maternal RNA' (**F**) and 'minor ZGA' genes (**G**) in early 2-cell embryos ($n = 30$). **H** Pearson analysis of correlation between H3K9cr and Pol II occupancy at promoter regions in early 2-cell embryos. **I** Metaplots showed average Pol II enrichment signals at TSS and TES for all genes and 'E2C-CRO' genes. **J** Metaplot of H3K9cr enrichment at TSSs of 'maternal RNA' and 'minor ZGA' genes in early 2-cell embryos. **K** Boxplots showed Pol II enrichment at TSSs of 'maternal RNA' and 'minor ZGA' genes in early 2-cell embryos, the boxplot composition (center line: median; box limits: quartile 1 and quartile 3, and whiskers showing the maximum and minimum values). **L** Volcano plot of show differential methylation between *siCtrl* and *siEchs1* early 2-cell embryos (calculated using methylKit). **M** Pearson analysis of correlation between H3K9cr density and DNA methylation level at gene promoter regions in early 2-cell embryos. **N, O** Different methylation levels in early 2-cell embryos at the global genome (**N**) and the promoter regions (**O**), the median is represented by a horizontal line in the violin plot. **P** Quantification of mislocalized mitochondria in early 2-cell embryos ($n = 12$). Scale bar: 20 μm. **Q, R** Examination of ROS ($n = 19$) and JC-1 ($n = 11$) levels in early 2-cell embryos. **S, T** Relative ATP levels (**S**) and mtDNA copy numbers (**T**) in early 2-cell embryos ($n = 20$). In (**F**), (**G**), (**H**), (**P**), (**Q**), (**R**), (**S**) and (**T**), data were presented as Mean ± SD of three independent replicates and examined by two-tailed unpaired Student's *t*-test. In (**B**), (**C**), (**K**), (**N**), and (**O**), data were examined by the Mann-Whitney U test. Source data are provided as a Source Data file.

Correlation analysis further revealed that the distance from H3K9cr-enriched SINE/B1 elements (with an enrichment index greater than 1) to the TSS of their most adjacent genes negatively correlated with both gene expression levels and Pol II enrichment at the TSS regions (Supplementary Fig. 10L). Consequently, we classified genes into three categories based on their transcript abundance: 'high', 'medium', and 'low' (Fig. 4O). Genes with higher transcript abundance exhibited greater Pol II enrichment (Fig. 4P). Histone Kcr enrichment at SINE/B1 elements located near the three gene groups did not show significant differences, suggesting that the intensity of histone Kcr at SINE/B1 elements adjacent to genes does not directly contribute to transcriptional activity (Fig. 4Q). In contrast, we observed that a shorter distance between SINE/B1 elements and their adjacent TSS regions correlated with higher gene expression levels (Fig. 4R). To investigate whether retrotransposon expression is universally activated through various histone acylations, we examined the effect of histone lactylation depletion using publicly available RNA-seq datasets. Our analysis revealed that loss of histone lactylation did not significantly affect retrotransposon expression in either early or late 2-cell embryos (Supplementary Fig. 10M, N).

Ribosomal DNA (rDNA) represents another class of regulatory repetitive elements that evolved into several subtypes during mammalian evolution and plays a pivotal role in regulating early embryonic development[39]. We identified a marked reduction in rRNA levels (Fig. 4S), accompanied by decreased translation activity in *Echs1*-knockdown 2-cell embryos, as assessed by HPG incorporation (Fig. 4T). Notably, inhibition of transcriptional activity using DRB did not alter rRNA expression (Supplementary Fig. 11A). This suggests that the reduction in rRNA levels in *Echs1*-knockdown embryos was not due to impaired ZGA but was directly influenced by histone Kcr.

In summary, our results demonstrate that *Echs1*-mediated histone Kcr is enriched at major ZGA loci, promoting transcription activation in late 2-cell mouse embryos, and play a positive role to ensure expression of repetitive elements.

Echs1-mediated histone Kcr specifically regulates mouse early developmental program

We next investigated the role of *Echs1*-mediated histone Kcr in regulating early embryonic development, focusing on its relationship with histone Kac. Specifically, we examined whether the reduction of histone Kcr caused by *Echs1* knockdown could be rescued, whether the phenotypic changes observed after *Echs1* knockdown were due to oocyte abnormalities, and whether the decrease in histone Kcr resulted from mitochondrial dysfunction.

First, we analyzed the distribution of H3K9cr and H3K27ac during the early and late 2-cell stages. We found that the distribution patterns of both modifications were highly similar, with enrichment at the TSS (only genes with H3K9cr peaks at TSS were analyzed) and intergenic regions (H3K9cr peaks at intergenic regions) (Supplementary Fig. 12A, B). In line with this, H3K9cr levels were positively correlated with H3K27ac signals (Supplementary Fig. 12C, D). Further correlation analysis revealed that both H3K9cr and H3K27ac were positively associated with Pol II and negatively associated with DNA methylation in the mouse genome during the early 2-cell stage (Supplementary Fig. 12E). As anticipated, ChIP-seq analysis of mouse early 2-cell embryos showed prominent overlap of H3K9cr peaks with active histone marks, including H3K27ac, H3K4me3, and H3.3, but not with the repressive histone mark H3K27me3 (Supplementary Fig. 12F).

Additionally, we exposed early 2-cell embryos to sodium crotonate and sodium acetate, and assessed their transcriptomes (Fig. 5A–D). RNA-seq results revealed that both chemicals enhanced transcriptional activity and inhibited maternal transcript degradation, with sodium crotonate having a significantly stronger effect than sodium acetate. Notably, the sodium crotonate treatment, but not sodium acetate, induced a marked increase in major ZGA at the early 2-cell stage (Fig. 5C, D). These findings suggest that histone Kcr and Kac work synergistically to promote transcriptional activity, with histone Kcr playing a more prominent role in enhancing ZGA activity.

To investigate the mechanism behind the concurrent reduction of histone Kac levels along with histone Kcr, we hypothesize that histone Kcr readers may interact with histone Kac writers. P300, an enzyme with both acetyltransferase and crotonyltransferase activities, is critical for early mouse embryogenesis[40]. AF9, a reader of crotonyllysine[41], is highly expressed in mouse oocytes (Fig. 2C). Our co-immunoprecipitation analysis confirmed an interaction between AF9 and P300 (Supplementary Fig. 13A). Moreover, knockdown of *Af9* at the GV stage in mice resulted in significantly reduced blastocyst formation (Supplementary Fig. 13B, C). Additionally, the levels of histone Kcr and the expression of minor ZGA genes were both diminished (Supplementary Fig. 13D, E).

To further examine the specific role of *Echs1*-mediated histone Kcr in early development, we created a Flag-tagged *Echs1* construct with synonymous mutations at the siRNA-targeted sequences. Ectopic expression of Flag-*Echs1* partially restored total ECHS1 protein levels (Fig. 5E), H3K9cr and H3K4cr levels (Fig. 5F, Supplementary Fig. 13F), minor ZGA gene expression (Fig. 5G), and H3K9ac levels (Fig. 5H). In addition, we supplemented the culture medium of *Echs1*-knockdown embryos with sodium crotonate or sodium acetate. Notably, the addition of sodium crotonate significantly improved blastocyst development and largely restored the expression of typical ZGA genes (Fig. 5I–K). In contrast, sodium acetate had minimal impact (Fig. 5I–K). These results support that the developmental failure observed upon *Echs1* knockdown is due to the impaired histone Kcr, rather than histone Kac.

We further investigated the effects of *Echs1* knockdown at the zygotic stage and observed a significant reduction in blastocyst formation (Fig. 5L, Supplementary Fig. 14A). This developmental arrest

https://doi.org/10.1038/s41467-025-60565-z

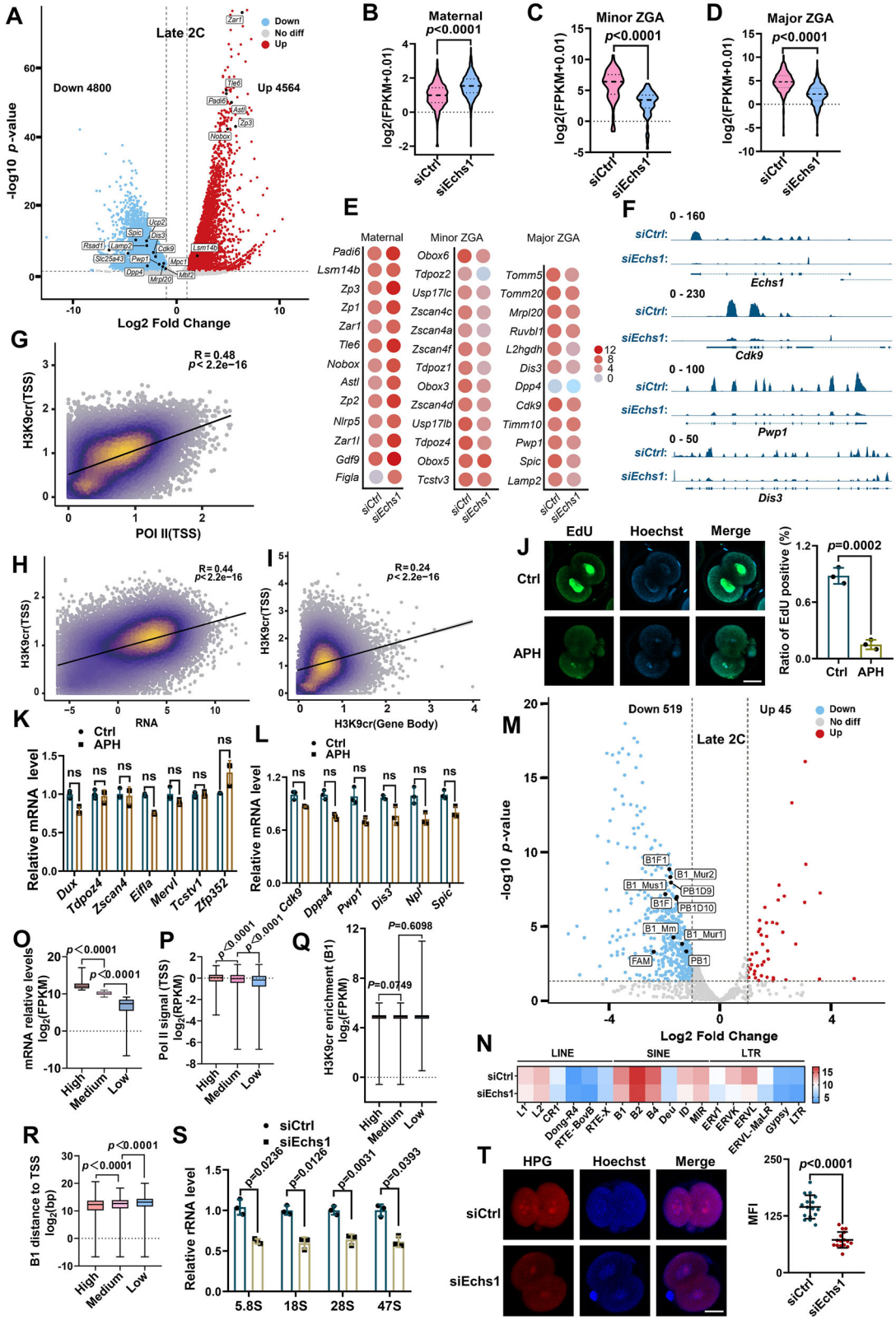

was associated with decreased histone Kcr levels and diminished ZGA gene expression (Fig. 5M, N). Additionally, we detected abnormalities in mitochondrial distribution and membrane potential (Fig. 5O and Supplementary Fig. 14B, C), as well as elevated ROS levels (Supplementary Fig. 14D). These findings indicate that the embryonic developmental defects resulting from *Echs1* knockdown at the GV stage were not limited to oocyte-specific effects.

To rule out the possibility that the reduction in histone Kcr after *Echs1* knockdown was due to mitochondrial dysfunction, we performed microinjections of siRNA targeting *Echs1* at the MII stage and assessed histone Kcr level and mitochondrial activity at the zygotic stage (Fig. 5P). The results revealed a substantial reduction in histone Kcr level and minor ZGA gene expression (Fig. 5Q, R), while mitochondrial integrity and ROS level remained unaffected (Fig. 5S,

Fig. 4 | Histone Kcr is essential for major ZGA and repetitive elements in late 2-cell stage in mice. A Volcano of transcript changes in *siEchs1* versus *siCtrl* late 2-cell embryos (*p*-value were calculated using DESeq2). **B**–**D** Violin plots of 'maternal RNA' (**B**), 'minor ZGA' (**C**) and 'major ZGA' (**D**) genes (GSE169632) expression in late 2-cell embryos. **E** Dotplots indicated representative genes expression in late 2-cell embryos. **F** Genomic browser view of RNA-seq results by IGV in late 2-cell embryos. **G** Pearson analysis between H3K9cr and Pol II density (GSE215813) at promoter in late 2-cell embryos. **H, I** Pearson analysis H3K9cr density between promoter and corresponding gene expression (**H**) or gene body (**I**) in late 2-cell embryos. **J** Images of EdU staining in 2-cell embryos treated with (APH)/without APH (Ctrl) ($n = 12$), scale bar: 20 μm. **K, L** qRT-PCR of 'minor ZGA' (**K**) and 'major ZGA' (**L**) genes expression in late 2-cell embryos ($n = 30$). Two-way ANOVA for analysis (Mean ± SD). **M** Volcano showed retrotransposon expression changes between *siEchs1* and *siCtrl* late 2-cell embryos (*p*-value were calculated using DESeq2), SINE/B1 family with changed expression were indicated. **N** Heatmap illustrated expression of retrotransposon subfamilies at late 2-cell embryo stage. **O** SINE/B1 adjacent genes were categorized into 'high', 'medium', and 'low' groups by transcription level in late 2-cell embryos. **P** Boxplot showing Pol II intensity at promoter in 'high', 'medium', and 'low' groups. **Q** Boxplot showing enrichment of H3K9cr at adjacent SINE/B1 elements of 'high', 'medium', and 'low' group genes. **R** Boxplot showing the distances between adjacent SINE/B1 elements and TSS of 'high', 'medium', and 'low' group genes. **S** qRT-PCR analysis the rRNA level in *siCtrl* and *siEchs1* late 2-cell embryos ($n = 30$). **T** HPG fluorescent staining in late 2-cell embryos ($n = 16$). Scale bar: 20 μm. In (**J**), (**S**) and (**T**), data were presented as Mean ± SD of three independent replicates and examined by two-tailed unpaired Student's *t*-test, ns indicates $P > 0.05$. In (**B**), (**C**) and (**D**), data were presented as Mean ± SD and examined by Mann-Whitney U test. In (**O**), (**P**), (**Q**) and (**R**), the boxplot exception (centre line: median; box limits: quartile 1 and quartile 3, and whiskers showing the maximum and minimum values). Source data are provided as a Source Data file.

Supplementary Fig. 14E–G). These data confirm that the primary impact of *Echs1* knockdown on ZGA gene expression is due to alterations of histone Kcr levels, rather than mitochondrial defects.

Enhancing histone Kcr level improves blastocyst formation of embryos from aged female mice

We observed that the intensities of both H3K9cr and H3K4cr were significantly lower in preimplantation embryos derived from aged female mice (12-month-old) compared to those from young mice (6-week-old) (Fig. 6A and Supplementary Fig. 15A). This suggests that reduced histone Kcr may contribute to the decline in the quality of embryos from maternally aged mice. We exposed mouse early embryos to serial dilutions of sodium crotonate and identified 15 μM as the most effective concentration for increasing histone Kcr levels (Supplementary Fig. 15B). Notably, supplementation with 15 μM sodium crotonate did not affect the development of early embryos from young female mice (Supplementary Fig. 15C). However, it significantly improved the blastocyst formation rate in embryos from aged female mice, increasing the rate from 17% to 33.7% (Fig. 6B, C). Consistent with this, histone H3K9cr levels and ZGA gene expression were markedly elevated in early 2-cell embryos from aged female mice exposed to sodium crotonate (Fig. 6D–F).

Next, we examined the impact of sodium crotonate exposure on the quality of early embryos from both young and aged female mice. At the blastocyst stage, we found that continuous exposure to sodium crotonate had no significant effect on embryos from the young group, but it increased the number of inner cell mass (ICM) and trophectoderm (TE) cells in embryos from aged females (Fig. 6G, H). IF analysis revealed no significant change in the fluorescence intensity of CDX2 in either group following sodium crotonate exposure, but OCT4 intensity was slightly higher in the aged group upon sodium crotonate exposure (Fig. 6G, I). These results suggest that supplementation with sodium crotonate enhances histone Kcr level, thereby improving the developmental quality of embryos from aged mice.

We then investigated the cause of reduced histone Kcr intensity with maternal aging. Our transcriptomic analysis revealed changes in the expression of crotonyl-CoA regulatory factors in early 2-cell embryos from aged female mice compared to those from younger females (Fig. 6J). Specifically, *Echs1* and *Cdyl* RNA levels were more abundant in early 2-cell embryos, with *Echs1* expression slightly decreasing and *Cdyl* expression slightly increasing in embryos from aged females. The IF results were consistent with the trends observed in transcript levels of *Echs1* and *Cdyl* (Supplementary Fig. 15D, E). Additionally, we observed reduced expression of typically transcribed genes at the early 2-cell stage in the aged group by RNA-seq (Fig. 6K). This suggests that *Cdyl* may play a key role in regulating histone Kcr and gene expression during early embryonic development, making it an interesting target for further investigation. To explore this, we knocked down *Cdyl* in early embryos from young female mice using the strategy similar to that used for *Echs1* deficiency (Fig. 2B and Supplementary Fig. 16A). However, we observed no significant change in the blastocyst formation rate following *Cdyl* knockdown (Supplementary Fig. 16B). Further analysis revealed a significant increase in H3K9cr level (Fig. 6L), along with elevated expression of typical minor ZGA genes (Fig. 6M, N, Supplementary Fig. 16C). Next, we applied the same knockdown strategy to embryos from aged female mice (Supplementary Fig. 16D). *Cdyl* knockdown led to an increase in the blastocyst formation rate and H3K9cr level, as well as elevated expression of minor ZGA transcripts (Supplementary Fig. 16E, F). These findings support that *Cdyl* negatively regulates histone Kcr level and transcriptional activity in early mouse embryos.

Given that *Echs1* and *Cdyl* have opposing effects on histone Kcr regulation in early mouse embryos, we investigated the blastocyst formation rate in embryos from young female mice with simultaneous knockdown of both *Echs1* and *Cdyl*. The results showed that, although the blastocyst formation rate and histone Kcr level were lower than those in the control group, they were significantly higher compared to the *Echs1*-only knockdown group (Supplementary Fig. 17A, B). Moreover, compared to the *Echs1* single-knockdown group, expression levels of maternal genes were lower in the double-knockdown group, whereas expression of minor ZGA genes increased (Supplementary Fig. 17C, D).

In summary, our findings demonstrate that enhancing histone Kcr levels promotes blastocyst formation in maternally aged embryos. This discovery could have important implications for improving assisted reproductive technologies by enhancing the quality of embryos from aged women.

Histone Kcr intensity is positively correlated with human ZGA activity

Our discovery that histone Kcr regulates transcription during early mouse embryonic development led us to investigate whether similar mechanisms are present in early human embryos. First, we analyzed the correlation between human ECHS1, CDYL, and ZGA genes using published RNA-seq data from human 8-cell embryos. Similar to findings in mouse embryos, we observed that ECHS1 positively correlates with typical human ZGA genes, such as ZSCAN4 and LEUTX, while CDYL shows a negative correlation with these genes (Fig. 7A). Co-staining of EU incorporation and H3K9cr signals in 4/8-cell human embryos revealed a positive correlation between nascent transcript synthesis and histone Kcr intensity (Fig. 7B). These results further support the idea that histone Kcr plays an active role in transcriptional activation during early human embryonic development.

IF staining of H3K9cr in early human embryos showed that nuclear histone Kcr signals increased from the 2-cell to the 4-8-cell stage, slightly decreased at the 16-cell stage, and then rose steadily thereafter (Supplementary Fig. 18A). To explore the genomic distribution of histone Kcr during human ZGA, we performed genome-wide H3K9cr

https://doi.org/10.1038/s41467-025-60565-z

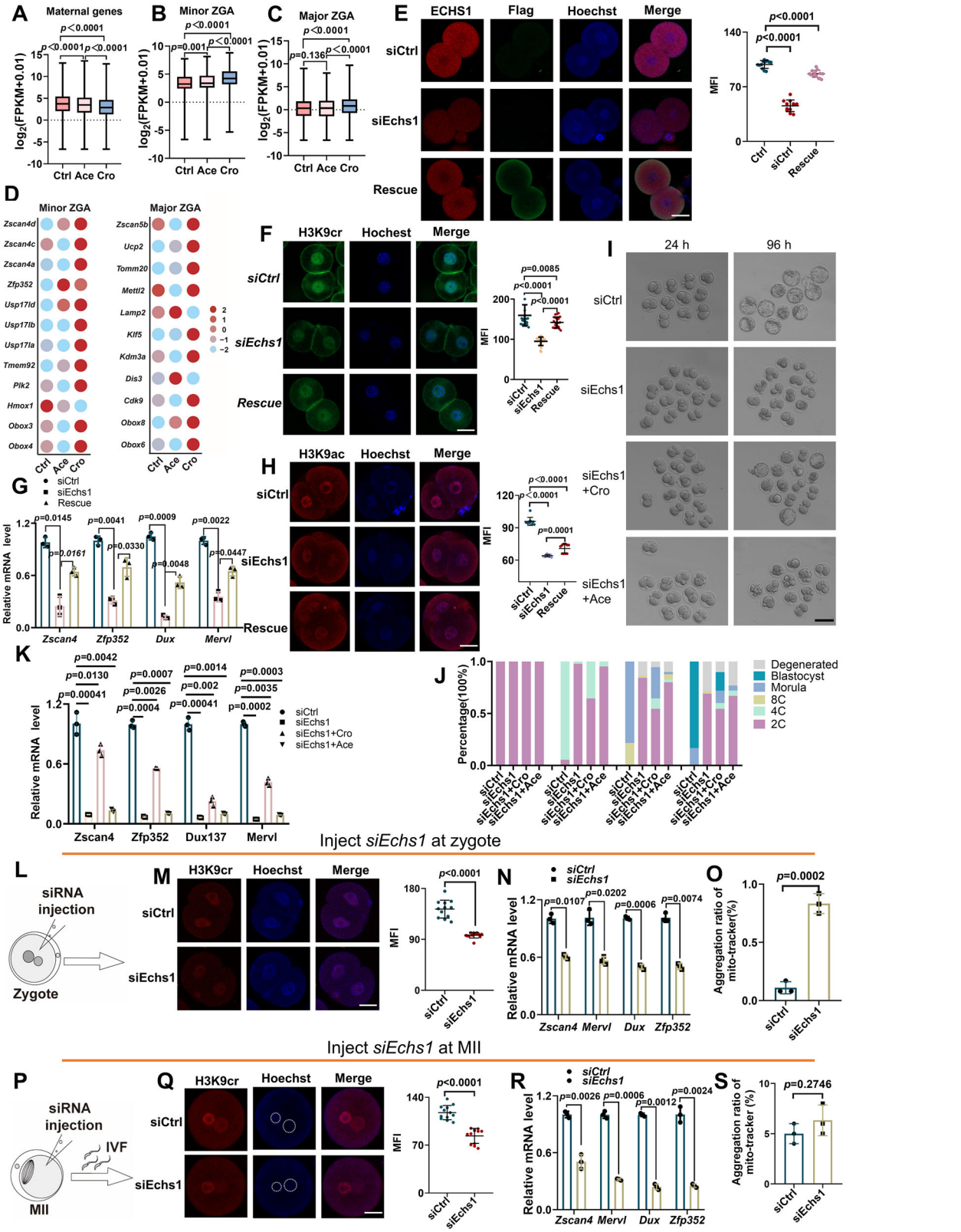

profiling on human early embryos, including 4-8-cell embryos, 16-cell embryos, and blastocysts (Fig. 7C, Supplementary Fig. 18B). Hierarchical clustering analysis distinctly separated samples from different developmental stages (Fig. 7D, Supplementary Fig. 18C). Genomic coverage analysis revealed that H3K9cr peaks were predominantly enriched at promoter regions, especially during the 4-8-cell stage in human early embryos (Fig. 7E). A Sankey diagram comparing H3K9cr CUT&Tag data from mouse and human samples at various developmental stages showed that a substantial number of genes with H3K9cr-enriched peaks at promoter regions in human 4-8-cell embryos were also identified in mouse 2-cell embryos, coinciding with the onset of ZGA (Fig. 7F). Further investigation into the distribution of H3K9cr in early human embryos revealed differential enrichment at retrotransposon elements across developmental stages (Supplementary

Fig. 5 | *Echs1*-mediated histone Kcr specifically regulates mouse early development beyond 2-cell stage. A–C Boxplots demonstrated transcript differences of 'maternal RNA' (**A**), 'minor ZGA' (**B**) and 'major ZGA' (**C**) genes (GSE169632) of early 2-cell embryos cultured without (Ctrl) or with sodium crotonate (Cro) /sodium acetate (Ace). The data (**A**–**C**) were examined by Mann–Whitney U test, the boxplot composition (centre line: median; box limits: quartile 1 and quartile 3, and whiskers showing the maximum and minimum values). **D** Dotplots indicated expression of representative genes in early 2-cell embryos. **E, F** Immunofluorescence staining and MFI of *ECHS1* protein (**E**) ($n = 12$) and H3K9cr (**F**) ($n = 22$) in *siCtrl*, *siEchs1* and exogenous *Echs1* co-expressed (rescued) embryos. Scale bars: 20 μm. **G** qRT-PCR result of representative 'minor ZGA' genes in *siCtrl, siEchs1* and rescued early 2-cell embryos ($n = 30$). **H** Immunofluorescence staining of H3K9ac in *siCtrl, siEchs1,* and rescued early 2-cell embryos ($n = 10$). Scale bars: 20 μm. **I** Representative developmental progression images of *siCtrl, siEchs1*, sodium crotonate rescued (*siEchs1*+Cro), and sodium acetate rescued (*siEchs1*+Ace) embryos. Scale bar: 100 mm. (**J**) Percentages of embryos at different stages ($n = 3$ independent replicates). **K** qRT-PCR result of representative 'minor ZGA' genes in *siCtrl, siEchs1*, *siEchs1*+Cro, and *siEchs1*+Ace early 2-cell embryos ($n = 30$). **L–O** Schematic (**L**) for *Echs1* knockdown in zygotes and experimental results (**M–O**). **M** Immunofluorescence staining and MFI of H3K9cr in early 2-cell embryos ($n = 12$). Scale bar: 20 mm. **N** qRT-PCR result of representative 'minor ZGA' genes in early 2-cell embryos ($n = 30$). **O** Aggregation ratio of mislocalized mitochondria in early 2-cell embryos ($n = 12$). **P–S** Schematic (**P**) for *Echs1* knockdown in MII oocytes and experimental results (**Q–S**). **Q** Immunofluorescence staining of H3K9cr of pronuclei observed in zygotes. Scale bar: 20 mm. **R** qRT-PCR result of representative 'minor ZGA' genes in *siCtrl* and *siEchs1* zygotes ($n = 30$). **S** Aggregation ratio of mislocalized mitochondria in zygotes ($n = 12$). In (**E**), (**F**), (**G**), (**H**), (**J**), (**K**), (**M**), (**N**), (**O**), (**Q**), (**R**) and (**S**), data were presented as Mean ± SD of three independent replicates and statistical evaluation was performed by two-tailed unpaired Student's *t*-test. Source data are provided as a Source Data file.

Fig. 18D). To assess the functional role of histone Kcr in human development, we supplemented the culture medium of 3PN human 1-cell embryos with sodium crotonate and cultured them for 32 h before collection (Supplementary Fig. 18E). Our analysis showed a significant increase in histone Kcr level in the sodium crotonate-treatment group, accompanied by enhanced expression of ZGA genes (Fig. 7G, H). These results support that the histone Kcr positively influences ZGA during early human embryonic development.

In conclusion, our findings demonstrate that histone Kcr enrichment in the human genome is closely linked to transcriptional activation, including ZGA, during early human embryonic development.

Discussion

The growing body of evidence underscores the critical role of histone modifications in regulating ZGA. These modifications include histone ubiquitination[42], acetylation[43], methylation[8], and SUMOylation[44]. Following fertilization, the embryo rapidly activates genome activation in two distinct waves in mice, marking the onset of embryonic development. The first, a minor ZGA, occurs from the zygote through the early 2-cell stage, while the major ZGA takes place at the late 2-cell stage[30,36]. In humans, ZGA is robustly observed during the 4-8-cell stage[45]. Histone Kcr plays a pivotal role in regulating transcriptional events associated with differentiation during early embryonic development[40], suggesting its involvement in initiating transcriptional activity in cleavage-stage embryos. In this study, we show that *Echs1* is the primary pathway for histone crotonyl-CoA synthesis during cleavage embryo development. We provide new insights into how *Echs1*-mediated histone Kcr activates embryonic transcription to support normal development. This finding aligns with a recent study demonstrating the essential role of histone Kcr in preimplantation embryo development. Specifically, the knockdown of the crotonyltransferase P300 at the zygotic stage led to a significant reduction in H3K18cr levels, which resulted in widespread transcriptomic dysregulation and developmental arrest during the 8-cell-to-morula transition[40]. Our study further reveals that inhibiting histone Kcr from the oocyte stage causes developmental arrest at the 2-cell stage. Consequently, our investigation primarily focuses on the regulatory functions of histone Kcr in the developmental program at 2-cell stage. Moreover, regulators controlling histone Kcr exist in multiple mammalian species and are widely expressed in different cell types, indicating that histone Kcr is involved in various developmental processes.

Echs1, also known as crotonase, catalyzes the conversion of 3'-hydroxybutyryl-CoA to crotonyl-CoA[13,46]. In tumor cells, ECHS1 functions as a negative regulator of histone Kcr, inhibiting tumor cell proliferation[15]. Additionally, a notable reduction in ECHS1 protein levels has been reported in the heart tissue of patients with cardiac hypertrophy[16]. Contrarily, studies on human stem cells have shown that ECHS1 acts as a crotonyl-CoA synthase, contributing to the generation of histone Kcr[13]. Consistently, our data demonstrate that *Echs1* is crucial for crotonyl-CoA synthesis in early embryos. Specifically, knocking down *Echs1* results in a decrease in histone Kcr levels, accompanied by a reduction in the expression of mitochondrial-related genes, disruption of mitochondrial morphology, a decline in mitochondrial membrane potential, and reduced ATP and mtDNA levels. Mitochondrial dysfunction during early development can impact ZGA timing and activity[47]. Further investigation is needed to understand how enzymes catalyzing histone Kcr and its "readers" contribute to transcriptional regulation in early embryos.

Fertilization initiates the establishment of a totipotent state through chromatin reprogramming, replacing the maternal program with the embryonic program[2,24,48]. During this reprogramming process, the embryonic genome gradually activates, promoting the degradation of maternal transcripts[49]. In mice, minor ZGA occurs early in the 2-cell stage, followed by the major ZGA at late 2-cell stage[50]. Our findings show a significant decrease in histone Kcr levels following *Echs1* knockdown, accompanied by pronounced changes in gene expression. These changes include reduced expression of both embryonic and mitochondrial genes, as well as increased expression of maternal RNA. Additionally, *Echs1* knockdown led to diminished Pol II enrichment at genic regions and histone Kcr sites in early embryos. Prior to ZGA, Pol II is preloaded at specific promoter regions but remains paused, a phenomenon known as promoter-proximal pausing[51]. Histone modifications and the activity of transcription factors can modulate the release of this paused state, enabling Pol II to commence transcription, with P300 functioning as a coactivator to facilitate chromatin opening and transcription activation[52]. Our study revealed that Pol II co-localized with histone Kcr in mouse 2-cell embryos, and we observed a positive correlation between Pol II and histone Kcr intensities in human 4-8-cell embryos. Notably, inhibiting Pol II elongation with DRB treatment resulted in decreased histone Kcr intensity and a reduction in ZGA gene expression. These results suggest that Pol II and histone Kcr work together to promote chromatin opening and transcription activation, crucial for normal embryonic development.

CDYL, a chromodomain Y-like transcription co-repressor and crotonyl-CoA hydratase, regulates the conversion of crotonyl-CoA to β-hydroxybutyryl-CoA, suppressing histone Kcr[53,54]. CDYL-mediated inhibition of histone Kcr is linked to transcriptional repression, the reactivation of sex chromosome-linked genes in round spermatids, and genome-wide histone replacement during spermatid elongation[22]. In alignment with these findings, our results show that histone Kcr levels significantly increase, along with a notable enhancement of ZGA gene expression, in embryos with *Cdyl* knockdown. Interestingly, we observed elevated *Cdyl* expression and decreased histone Kcr levels in embryos derived from aged females. These results suggest that, in the context of clinical embryonic development from oocytes of older women, targeting *Cdyl* with specific inhibitors may boost histone Kcr levels and improve embryo quality.

https://doi.org/10.1038/s41467-025-60565-z

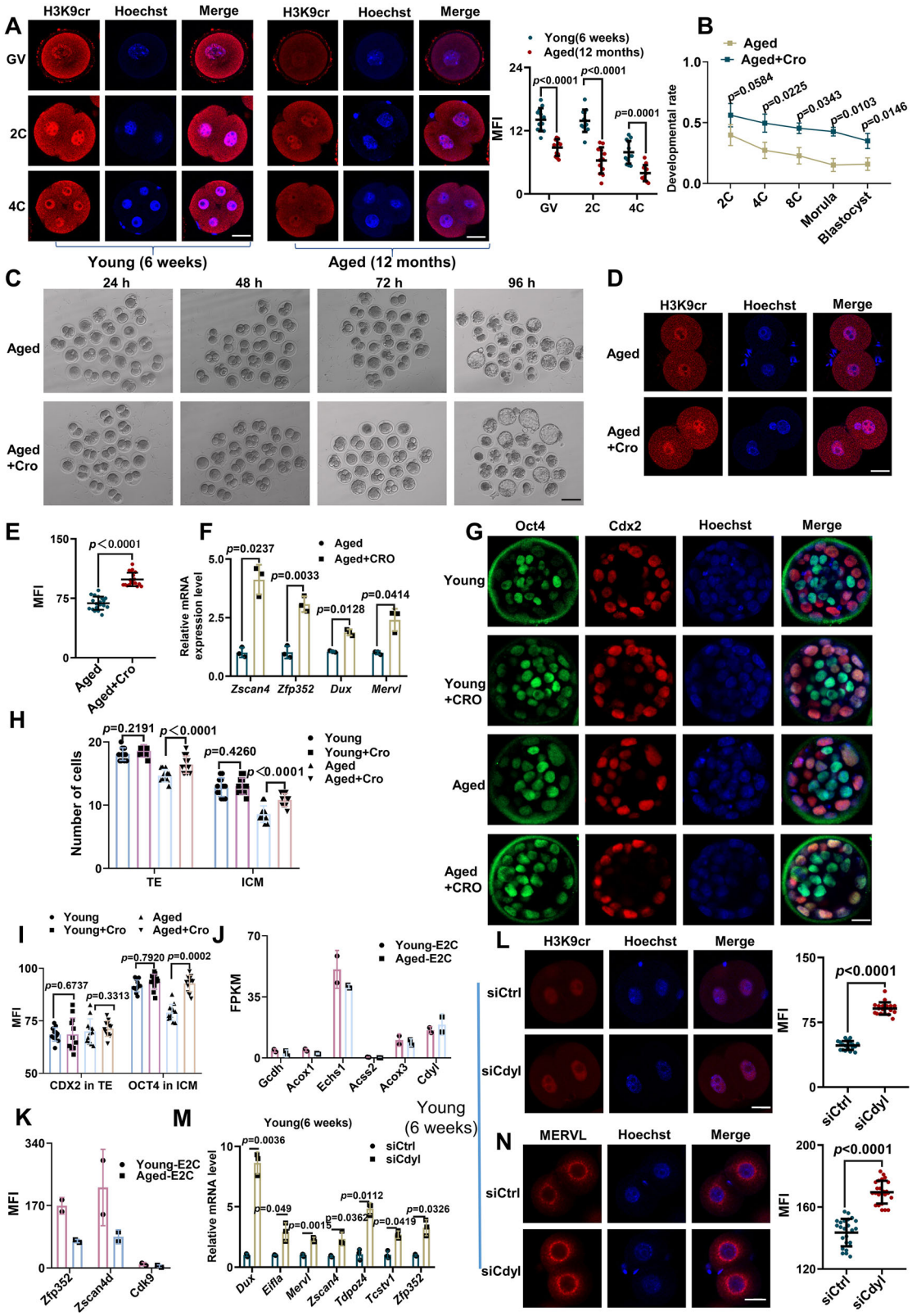

Evidence has shown that repetitive elements play essential roles in regulating ZGA and preimplantation development. For instance, the totipotency factor *Nr5a2* has been shown to initiate ZGA by binding to the SINE B1/Alu element in the cis-regulatory regions of ZGA genes[55]. In our study, a reduction in *Echs1*-mediated histone Kcr led to a significant decrease in the expression of repetitive elements, including LTR, LINE, and SINE, at the late 2-cell stage in mice, with a particularly strong impact on SINE/B1 family members. These SINE/B1 elements may promote transcription by functioning as upstream expression cassettes that drive transcription initiation or as enhancers that activate adjacent genes. Notably, our data revealed a negative correlation between the distance of SINE/B1 elements from the adjacent TSS and gene expression levels. A previous study suggested that small RNAs derived from SINE/B1 elements contribute to gene silencing in

Fig. 6 | Exogenous crotonate improves the blastocyst formation rate in embryos derived from aged female mice. A Immunofluorescence staining and MFI of H3K9cr in GV oocytes, 2-cell embryos and 4-cell embryos of maternally young/aged mice ($n = 12$). Scale bars: 20 μm. **B** Percentages of embryos at different stages were presented as Mean ± SD ($n = 3$ independent replicates), data statistical evaluation was performed by two-way ANOVA. **C** Representative developmental progression images of maternally aged embryos which were cultured in KSOM medium with (Aged+Cro) or without sodium crotonate (Aged) ($n = 3$ independent replicates). Scale bars: 100 μm. **D, E** Immunofluorescence staining (**D**) and MFI (**E**) of H3K9cr in 'Aged' and 'Aged+Cro' early 2-cell embryos ($n = 19$). Scale bars: 20 μm. **F** qRT-PCR results of representative 'minor ZGA' genes in 'Aged' and 'Aged+Cro' early 2-cell embryos ($n = 30$). **G** Representative Oct4 and Cdx2 immunofluorescence images and quantification of maternally young/aged embryos which cultured with or without sodium crotonate. Different lineage cells were defined by fluorescence signals: inner cell mass (ICM, $Oct4^+/Cdx2^-$) and trophectoderm (TE, $Cdx2^+$). Scale bars: 20 μm. **H** Graphs showed the statistical number of TE and ICM cells respectively in maternally young/aged blastocysts cultured with or without sodium crotonate ($n = 12$). **I** Graphs showed the MFI of TE and ICM respectively in maternally young/aged blastocysts which cultured with or without sodium crotonate ($n = 12$). **J–K** Bar charts compared expression differences (GSE241388) of histone crotonylation regulators (**J**) and ZGA genes (**K**) between maternally young/aged mouse early 2-cell embryos, expression of either *Cdyl* or *Echs1* was not significantly changed ($P > 0.05$ by DESeq2). **L** Immunofluorescence staining and MFI of H3K9cr in maternally young early 2-cell embryos ($n = 19$) with (*siCdyl*) or without (*siCtrl*) *Cdyl* knockdown. Scale bars: 20 μm. **M** qRT-PCR analysis showed expression changes of representative 'minor ZGA' genes in maternally young *siCdyl* early 2-cell embryos ($n = 30$). **N** Immunofluorescence staining and MFI of *MERVL* protein in maternally young *siCdyl* and *siCtrl* early 2-cell embryos ($n = 24$). Scale bars: 20 μm. In (**A**), (**E**), (**F**), (**H**), (**I**), (**L**), (**M**) and (**N**), data were presented as Mean ± SD of three independent replicates and statistical evaluation was performed by two-tailed unpaired Student's *t*-test. Source data are provided as a Source Data file.

preimplantation mouse embryos[56]. Based on this, we propose that in mouse 2-cell embryos, the increased maternal RNA levels observed upon *Echs1* knockdown may partly result from reduced histone Kcr levels and the suppression of SINE retrotransposon expression.

It was reported that exogenous crotonic acid supplementation induced histone Kcr, activated 2-cell genes such as *Zscan4*, and promoted the generation of chemically induced pluripotent stem cells[57]. Similarly, our findings show that an optimal dose of sodium crotonate enhances histone Kcr, thereby stimulating ZGA in both early mouse and human embryos. Furthermore, the developmental arrest caused by decreased histone Kcr due to *Echs1* deficiency was partially rescued by exogenous sodium crotonate supplementation. In addition, during embryonic development in aged female mice, sodium crotonate significantly improved the blastocyst formation rate. Interestingly, previous studies have shown that crotonate can mitigate aging in differentiated glioblastoma cells by enhancing histone Kcr[15], supporting our finding that histone Kcr plays a crucial role in improving the quality of maternally aged embryos and may enhance fertility in aged females. Our study highlights the clinical potential of crotonate as a promising intervention to optimize reproductive outcomes in older women, whether through natural conception or assisted reproductive technologies.

In summary, we have mapped the dynamic genome-wide distribution of histone Kcr during early embryonic development in both mice and humans and explored its role in transcription activation in early mammalian embryos (Fig. 8). Specifically, reducing histone Kcr by inhibiting *Echs1* expression led to decreased expression of ZGA genes and repetitive elements in early mouse embryos, causing developmental arrest at the 2-cell stage. Conversely, enhancing histone Kcr in embryos from aged female mice promoted blastocyst formation, suggesting that histone Kcr is a potential target for addressing developmental issues linked to maternal aging. Overall, our findings offer valuable insights into the mechanisms of transcriptional regulation during early embryonic development and underscore the functional significance of histone Kcr.

Methods

Animals

Animal procedures were approved by the Institutional Animal Care and Use Committee of Tongji Medical College, Huazhong University of Science and Technology (IACUC Number 4096). The animal handling and experimental protocols were designed according to the Guide for the Care and Use of Laboratory Animals.

ICR mice were used in this study and were purchased from Bainte Biotechnology Company (Hubei, China). All mice were kept in pathogen-free facility with constant and carefully controlled environment (22-24 °C, 46%-65% humidity) of Huazhong University of Science and Technology, including a regular 12-h day/night cycle of light and adequate food. 6-week-old female mice were used in the young group, 12-month-old female mice were used in the aged group, and sperm were collected from 10-week-old male ICR mice.

Human embryo collection with ethical approval

The use of human gametes in this study complies with all relevant ethical regulations, including the Human Biomedical Research Ethics Guidelines (issued by the National Health Commission of the People's Republic of China, 2016), the Guidelines for Stem Cell Research and Clinical Translation (ISSCR, 2016), and the Human Embryonic Stem Cell Research Ethics Guidelines (issued by the China National Center for Biotechnology Development, 2003). Human preimplantation embryos utilized in the study were obtained from the Reproductive Medical Center, Renmin Hospital of Wuhan University. All experiments involving human early embryos were conducted ethically in accordance with the CEIC (Ethics Committee for Clinical Research) of the HUST (S207) and were conducted in accordance with the principles of the Declaration of Helsinki.

The human zygotes used in this study were derived from clinically abnormal three-pronuclei (3PN) embryos. The 4-cell, 8-cell, morula, and blastocyst-stage embryos were all voluntarily donated for scientific research by patients who had successfully given birth and had surplus frozen oocytes. Prior to signing written informed consent, all patients were thoroughly informed about the purpose of the study and the intended use of the donated samples. The donation was entirely voluntary, and no financial compensation was provided. Donors were women aged between 24 and 35 years. Written informed consent was obtained from all embryo donors. Vitrification and thawing of preimplantation embryos were performed according to manufacturer's instruction (Vitrification kit & Thawing kit, KITAZATO Corporation, Japan).

Generally, following the collection of vitrified human embryos, the embryos were cryopreserved in liquid nitrogen and were transferred for thawing later. The thawing protocol was conducted as follows: embryos were initially immersed in pre-warmed (37 °C) Thawing Solution (TS) for 1 min, followed by sequential equilibration in room temperature solutions, then transferred to Dilution Solution (DS) for 3 min and Washing Solution 1 (WS1) for 5 min, and finally to Washing Solution 2 (WS2) for an additional 5-min incubation at room temperature. Post-thawing recovery was assessed morphologically using a capillary glass pipette to select viable embryos with intact cellular structures and normal developmental morphology. Selected embryos were cultured in G1 medium under standardized conditions: 37 °C in a humidified atmosphere containing 5% CO_2. Embryonic developmental progression was monitored until reaching specific cleavage stages.

Acquisition of mouse oocytes and in vitro maturation (IVM)

To collect GV stage oocytes, ovaries were obtained from female ICR mice aged 6 weeks. The ovaries were mechanically clipped using

https://doi.org/10.1038/s41467-025-60565-z

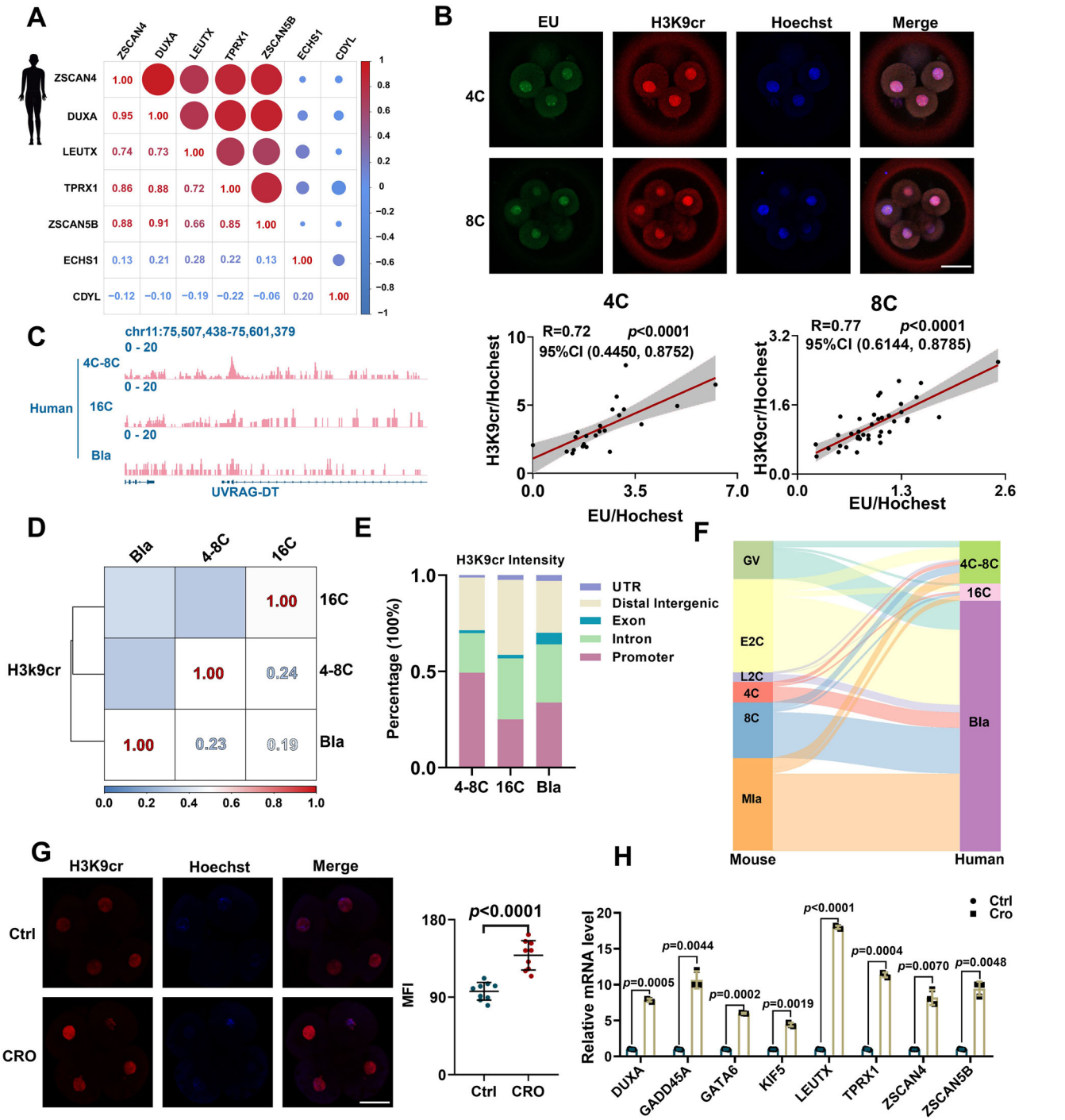

Fig. 7 | Enrichment of histone Kcr during early human embryonic development. **A** Pearson correlation analysis on expression of human ZGA genes, ECHS1 and CDYL, using reported single-cell RNA-seq data of human 8-cell stage embryos (GSE36552, GEO repository, NCBI). **B** Immunofluorescence co-staining of EU and H3K9cr in human 4-cell and 8-cell embryos, and Pearson correlation analysis demonstrated positive correlation between EU and H3K9cr fluorescence signals in both 4-cell and 8-cell embryos, with shaded areas representing the 95% confidence intervals ($n = 24$). Scale bars: 20 μm. **C** Genome browser view of representative H3K9cr signals in cleavage embryos and blastocyst by IGV. **D** Spearman correlation analysis of genome-wide H3K9cr occupancy in various developmental stages of human embryos. **E** The percentages of H3K9cr peaks assigned to the different genomic regions including promoter, intron, exon, UTR, and intergenic regions across various developmental stages. **F** Sankey diagram comparing genes with H3K9cr peaks at promoter regions in different developmental stages between human and mouse, with the width of the connecting line being proportional to the strength of the correlation. **G** Immunofluorescence staining and mean fluorescence intensity of H3K9cr in human 3PN embryos which cultured in G1 medium with (CRO) or without (Ctrl) sodium crotonate for 32 h from 1-cell stage ($n = 9$). Scale bars: 20 μm. **H** qRT-PCR result of representative 'minor ZGA' genes in human 8-cell embryos which cultured in G1 medium with (CRO) or without (Ctrl) sodium crotonate ($n = 20$). The data of qRT-PCR were presented as Mean ± SD of three independent replicates. The data statistical evaluation of qRT-PCR and fluorescence intensity quantification was performed by two-tailed unpaired Student's *t*-test. Source data are provided as a Source Data file.

https://doi.org/10.1038/s41467-025-60565-z

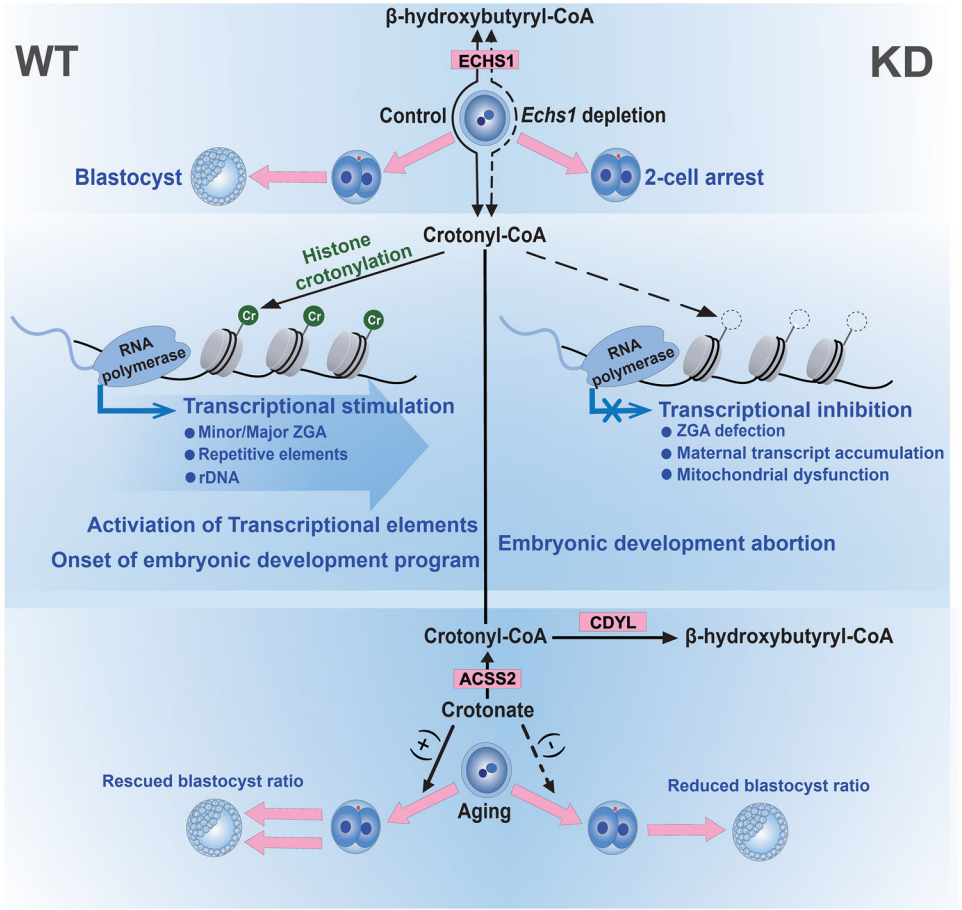

Fig. 8 | Working model illustration of *Echs1*-mediated histone crotonylation regulating early embryo development. *Echs1* supports early embryo development by regulating crotonyl-CoA synthesis to generate histone crotonylation. Under physiological condition, *Echs1* sustains normal level of crotonyl-CoA in early embryos, ensuring sufficient histone crotonylation for transcription activation at ZGA genes, retrotransposon elements, and rDNA loci, thereby ensuring normal early embryo development. When *Echs1* is deficient, histone crotonylation level decreases, ZGA event fails, maternal mRNA degradation is impaired, mitochondrial dysfunction occurs, and embryonic development is arrested. Additionally, the addition of exogenous crotonate to the culture medium of embryos from aged female mice improves blastocyst formation. In summary, *Echs1*-mediated histone crotonylation is crucial for transcription activation of ZGA genes and repetitive elements to support early embryo development.

ophthalmic scissors. GV oocytes were collected using homemade capillary glass tubes under a stereomicroscope, and placed in paraffin oil-covered M2 medium containing 2.5 μm Milrinone at 37 °C under 5% CO_2. For in vitro maturation (IVM), GV oocytes were transfer to M16 medium at 37 °C in a 5% CO_2 incubator for 16 h.

For collection of MII oocytes, 10 IU pregnant horse serum gonadotropin (PMSG) was injected intraperitoneally to induce ovulation in 6-week-old female ICR mice, followed by injection of 10 IU human chorionic gonadotropin (hCG) 48 h later. Cumulus-oocyte complexes (COCs) were collected from the juxtaperitoneal part of the mouse oviduct 14 h after hCG injection, and the oocytes were digested with hyaluronidase (Nanjing Aibei Biotechnology, M2215). Oocytes were then washed several times with M2 medium for subsequent experiment.

cRNA construct and in vitro Transcription

cDNA of *Echs1* cloned from mouse ovary was introduced into pVAX1 plasmid. To avoid recognition by siRNA, synonymous mutations of *Echs1* sequence was introduced by the QuikChange II site-directed mutagenesis kit (Agilent, USA) and the mutations were confirmed by sanger sequencing. Detailed mutated sequences are displayed in the Supplementary Table 1.

Subsequently, capped cRNA was synthesized from linearized plasmids using the mMESSAGE mMACHINE T7 Ultra kit (Thermo Fisher Scientific, USA) and purified through precipitation with LiCl, followed by dissolution in nuclease-free water and storage at -80 °C.

Microinjection

For knockdown experiment, siRNAs were designed (Genepharma, China) to target different regions of mouse *Acss2*, *Echs1*, or *Cdyl* mRNA, respectively. A non-targeting siRNA was used as negative control. Using Nikon Eclipse TE300 Inverted Microscope (Nikon, Japan), 5-10 pl of siRNA was injected into the cytoplasm of GV oocytes. To examine siRNA efficiency in oocytes, injected GV oocytes were incubated with 2.5 μm Milrinone for 48 h, followed by detection of mRNA/protein levels. To collect early embryos, injected GV oocytes were incubated with 2.5 μm Milrinone for 18 h, followed by in vitro maturation for fertilization. For the rescue experiment, 0.5–1.0 μg/μl cRNA encoding *Echs1* gene with synonymous mutation sites was co-injected with siRNA into cytoplasm of GV oocytes. The siRNA sequences are shown in Supplementary Table 2.

In vitro Fertilization (IVF) and Early Embryo Collection

For IVF, the caudal epididymis was mechanically removed from the testis to collect spermatozoa which were incubated in HTF medium for capacitation and added to the drop containing MII oocytes. Fertilized oocytes were then transferred to KSOM (Nanjing Aibei Biotechnology, China) medium. Early embryonic development was monitored at

specific time points, and embryos were collected at distinct stages of development. Zygotes were collected at 8 h post-fertilization, early 2-cell embryos were collected at 22 h post-fertilization (day 1.0), late 2-cell embryos were collected at 32 h post-fertilization (day 1.5), 4-cell embryos were collected at 48 h post-fertilization (day 2.0), 8-cell embryos were collected at 60 h post-fertilization (day 2.5), morula were collected at 72 h post-fertilization (day 3.0), and blastocysts were collected at 96 h post-fertilization (day 4.0–4.5). Each exposure experiment and the corresponding immunofluorescence analysis were performed using the same batch of female mice. For IVF, each young female mouse yielded 15-25 oocytes, and each aged female mouse yielded 5-10 oocytes. At least 10 oocytes/embryos were used per replicate. All embryos were collected using a sterile pipette under a dissecting microscope to ensure precise timing and minimize contamination.

Embryonic pharmacological treatment

Zygotes at 4 h post-fertilization were transferred into KSOM medium containing sodium crotonate, sodium acetate, sodium lactate, and β-hydroxybutyrate respectively (at a concentration of 15 μM), and then collected at 22 h post-fertilization to detect histone modifications and mRNA levels of specific genes. To study the effect of DRB (MERCK, Germany) on embryonic development, zygotes at 4 h post fertilization were transferred to KSOM medium containing 80 μM DRB and collected at 22 h post-fertilization for further analysis. To investigate the effect of APH on embryonic development, early 2-cell embryos were collected at 22 h post-fertilization and then transferred to KSOM medium containing 4 μg/ml APH, and cultured for 6 h before being collected for further analysis.

Immunofluorescence and confocal microscopy

Oocytes or embryos were fixed with 4% paraformaldehyde for 30 min at room temperature, followed by permeabilization with PBS containing 1% Triton X-100 for 10 min, or by direct permeabilization and fixation with a mixture containing 1% Triton X-100 and 4% paraformaldehyde in equal proportions. Next, the samples were blocked with 1% BSA for 1 h, and then incubated with primary antibodies at 4 °C overnight. After washing with PBS wash solution containing 0.1% Triton X-100 and 0.01% Tween, samples were incubated with secondary antibodies and 10 μg/ ml Hoechst 33342 for 2 h at room temperature. The samples were promptly imaged by confocal microscope (Zeiss LSM 900 META). Fluorescence Intensities were analyzed by ZEN lite 2012 (Zeiss) and Image J software (National Institutes of Health, USA). Fluorescence intensity quantification are presented as Mean ± SD, and identified as mean fluorescence intensity (MFI). The primary and secondary antibodies used are listed in Supplementary Table 3.

In this study, to minimize batch effects, when comparing the immunofluorescence staining intensity of the same batch, embryos from the same batch of mice, all stimulated for superovulation at the same time point, were exposed to drugs. Fixation, permeabilization, blocking, staining, photographing and analysis were then carried out simultaneously or in parallel under the same conditions.

Co-immunoprecipitation (Co-IP)

NIH-3T3 mouse embryonic fibroblasts obtained from ATCC were cultured in DMEM supplemented with 10% FBS (Hyclone, SH30396.03) and 1% penicillin-streptomycin (Thermo Fisher Scientific) at 37 °C under 5% CO_2. Collected mouse cells were washed twice with ice-cold PBS and lysed in NP-40-based lysis buffer (50 mM Tris-HCl pH 8.0, 150 mM NaCl, 1% NP-40, 1 mM EDTA) containing protease and phosphatase inhibitor cocktails. Lysates were incubated on ice for 30 min with gentle agitation, followed by centrifugation at 14,000 × *g* for 15 min at 4 °C. The supernatants were pre-cleared with Protein A/G magnetic beads (Vazyme, PB101-01) for 1 h. For immunoprecipitation, 2 μg of specific antibody (anti-P300 antibody, Abcam, ab275378; anti-AF9 antibody, Proteintech, 12825-1-AP) was incubated with lysate overnight at 4 °C with rotation. Antibody-protein complexes were captured by adding Protein A/G beads for 2 h at 4 °C, followed by three washes with high-stringency buffer (50 mM Tris-HCl pH 7.4, 300 mM NaCl, 0.1% NP-40). Immunoprecipitated samples were resolved by SDS-PAGE and analyzed via western blot using indicated antibodies. All experiments were independently repeated for three times. The primary and secondary antibodies used were listed in Supplementary Table 3.

Western blot

Approximately 300 oocytes or early embryos were lysed with the 50 μl RIPA buffer containing protease inhibitors. The samples were separated by SDS-polyacrylamide gel electrophoresis and transferred to a polyvinylidene difluoride (PVDF) membrane which was blocked with Tris-buffered saline tween (TBST) containing 5% skimmed milk and incubated with primary antibodies at 4 °C overnight. After washing and incubation with secondary antibodies, membrane signals were detected using an enhanced chemiluminescence detection system (BIO-RAD, ChemiDoc MP Imaging System), and band intensity values were quantified using Image J software. The primary and secondary antibodies used were listed in Supplementary Table 3.

Active mitochondrial staining

Embryos were washed with M2 twice, and placed in pre-equilibrated 500 nmol/l MitoTracker Red CMXRos (Beyotime, China) for incubation for 30 min at 37 °C. After washing with M2 medium, embryos were stained with 10 μg/ml Hoechst 33342 (Sangon Biotech) in M2 medium for 20 min. Embryos were examined by a confocal microscope for fluorescence intensity and images were analyzed using ZEN lite 2012 software.

Reactive Oxygen Species (ROS) Measurement

When comparing ROS content of the same batch, oocytes or embryos were collected and processed from mice of the same batch, subsequently exposed to dye simultaneously or parallelly under the same conditions. Total ROS content in oocytes and embryos was quantified using a ROS assay kit (Beyotime, China). Early 2-cell embryos or oocytes were placed in M2 medium containing DCFH-DA and covered with paraffin oil. The samples were then incubated at 37 °C for 25 min, washed with M2, and immediately imaged by the confocal microscope.

Mitochondrial Membrane Potential (MMP), Endoplasmic Reticulum (ER), and Lysosome Detection

To detect alterations of MMP, ER and lysosomal localization, oocytes or embryos were placed in M2 dilutions of JC-1, ER-Tracker Red and Lyso-Tracker Red medium, respectively, covered with paraffin oil, and incubated for 30 min at 37 °C. Subsequently, the samples were washed with fresh M2 medium for three times with 5 min each, and immediately imaged under a confocal microscope. In JC-1 staining, the ratio of red to green fluorescence intensity indicated the change in mitochondrial membrane potential. Embryos used for comparison were collected and processed from mice of the same batch, subsequently exposed to dye simultaneously or treated in parallel under the same conditions.

5-Ethynyl Uridine Staining

Global transcriptional assays were performed using the EU nascent RNA detection kit (RIBOBIO, China) according to the manufacturer's instructions. Generally, embryos were incubated with 1 mM EU at 37 °C for 2 h. Samples were then fixed with 4% PFA for 30 min, permeabilized with 0.5% Triton X-100 for 10 min, incubated with Apollo mix for 30 min, and washed for three times with PBS before staining with 10 μg/mL Hoechst 33342 for DNA staining. The samples were imaged under a confocal microscope and the fluorescence signal was analyzed to assess nascent RNA synthesis.

Embryos used for comparison of 5-Ethynyl Uridine signal were collected and processed from mice of the same batch, subsequently exposed to dye simultaneously or treated in parallel under the same conditions.

Cell proliferation detection

The detection of EdU signaling was conducted in accordance with the instructions provided by the manufacturer of BeyoClick EdU Cell Proliferation Kit with Alexa Fluor 488 (Beyotime, China). Briefly, embryos at 20 h post fertilization were cultured in KSOM containing 10 μM EdU for 3 h. Next, embryos were fixed in 4% paraformaldehyde for 15 min and permeabilized with 0.5% Triton X-100 for 15 min. The embryos were then incubated in the click reaction buffer for 30 min and stained with 10 μg/ml Hoechst 33342 and imaged using a fluorescence microscope. Embryos used for comparison of EdU signal were collected and processed from mice of the same batch, subsequently exposed to dye simultaneously or treated in parallel under the same conditions.

Detection of protein synthesis

Detection of Protein Synthesis was conducted using the Click-iT HPG Alexa Fluor 594 Protein Synthesis Assay kit (Thermo Fisher Scientific, USA). Generally, embryos were cultured with 50 μM HPG (L- Homopropargylglycine) for 2 h. Subsequently, the embryos were transferred to M2 medium for 30 min at 37 °C. Then the embryos were washed with PBS and stained with 10 μg/mL Hoechst 33342. The HPG signals were imaged using a confocal microscope. Oocytes or embryos used for comparison of HPG signal were collected and processed from mice of the same batch, subsequently exposed to dye simultaneously or treated in parallel under the same conditions.

Measurement of ATP level

ATP levels were quantified using the ATP assay kit (Beyotime, China). Generally, 20 embryos were lysed in lysis buffer containing 20 mM Tris (pH 7.0), 0.9% Nonidet P-40, and 0.9% Tween−20. This solution was prepared according to the standard method supplied by the manufacturer and placed on ice. For the ATP assay, 100 μl of the standard solution and 5 μl of the sample were added to each well of a 96-well plate and allowed to equilibrate for one min prior to measurement. Three replicates were set up for each sample. A standard ATP curve was set up for each assay based on five ATP concentrations of 0, 0.1, 0.5, 1.0, 10, and 50 pmol, and the ATP content was calculated using the linear regression equation of this standard curve.

RNA extraction and quantitative real-time PCR (qRT-PCR)

Total RNA was extracted from 50 oocytes or 50 embryos using Trizol reagent (Ambion, USA) following the manufacturer's instructions. Complementary DNA was obtained using the HiScript II Q RT SuperMix (Vazyme, China), and qRT-PCR experiments were conducted using Taq Pro Universal SYBR qPCR Master Mix (Vazyme, China) on Quantagene q225 qPCR system (Kubo Technology, Beijing). Each experiment was independently repeated for at least three times, gene expression was normalized to *Gapdh* and evaluated using the ΔΔCT method (the relative expression level of genes in control was set as 1.0). In this study, to minimize batch effects, when comparing the gene expression of the same batch, oocytes or embryos were collected from mice of the same batch and processed simultaneously or treated in parallel under the same conditions. The primers used were listed in Supplementary Table 4.

Mitochondrial DNA (mtDNA) copy number assay

To extract mtDNA, approximately 20 2-cell embryos were added to 10 μl of lysis buffer (50 mM Tris-HCl pH 7.6, 0.5% Triton X-100, with Proteinase K at a concentration of 200 μg/ml) and incubated for 2 h at 55 °C. The products were diluted and subjected to qRT-PCR to determine the relative level of mtDNA.

Low-input RNA sequencing and data analysis

Three sets of replicates were established in both the experimental and control groups, and a total of 8-12 mouse early embryos were obtained in each replicate group for library preparations. Briefly, the embryos were collected in lysis components with ribonuclease inhibitors. Following amplification by the Smart-Seq2 method (Takara, Japan), first-strand cDNA synthesis was conducted using Oligo-dT primers during reverse transcription. cDNAs were then amplified by PCR and purified by magnetic beads, and cDNA production were assessed using a Qubit 3.0 Fluorometer and an Agilent 2100 Bioanalyzer. Next, the cDNA was fragmented and subjected to Illumina TruSeq library preparation (Illumina, USA). The qualified libraries were loaded onto the Illumina HiSeq platform for PE150 sequencing (BGI, China). 2-3 replicates were performed for each group. The raw sequencing data was processed using cutadapt v1.16 (https://cutadapt.readthedocs.io) to remove adapters and perform quality trimming with default parameters. The trimmed reads were then aligned to the mouse reference genome (mm10) or the human reference genome (hg19) using STAR (v2.5.3b) software with the default settings. The differential expression of genes was evaluated using the R package DESeq2 (v1.24.0). Genes were classified differentially expressed as down-regulated/decreased with $\log_2$ fold change < -1 ($P < 0.05$) while up-regulated/increased with $\log_2$ fold change >1 ($P < 0.05$). RSEM was employed to calculate FPKM values for each gene (Supplementary Data 1). TEtranscript with default parameters was used to obtain counts for different transposable elements (TEs). GO enrichment and KEGG pathway enrichment analyses were conducted using the DAVID website[58,59].

CUT&Tag Library Preparation and Dataset Analysis

CUT&Tag libraries were generated using the Hyperactive Universal CUT&Tag Assay Kit for Illumina Pro (Vazyme, China) according to the manufacturer's protocol with indicated antibodies. Mouse oocytes or embryos (GV oocytes, early 2-cell embryos, late 2-cell embryos, 4-cell embryos, 8-cell embryos and morula) and human embryos (4-8-cell embryos,16-cell embryos and blastocysts) were used as starting materials for library preparation. A total of 100-200 embryos were used in each library preparation. Generally, cells were bound to equilibrated ConA Beads Pro for permeabilization, followed by the addition of the primary antibody and secondary antibody. Next, pA/G-Tnp Pro was added to the samples for tagmentation. The libraries were purified with VAHTS DNA Clean Beads (Vazyme, China) for PE150 sequencing using Illumina HiSeq 3000 (Annoroad Gene Technology, China). 2 replicates were performed for each group.

Raw reads were subjected to processing using Trim Galore (v0.6.4) with the specified parameters '−q 25 −stringency 5− length 20 −paired −phred33', with the objective of removing poor-quality base sequences. The processed data were then aligned to the mouse reference genome (mm10) and human reference genome (hg19) using Bowtie2 (version 2.4.2) with the default settings, and peaks were identified using MACS2 (v2.2.7.1)[60]. The bedgraph files were converted first to bigwig files using the UCSC Genome Browser tool bedGraphToBigWig[61] and then displayed in the Integrative Genomics Viewer (IGV). Genomic coordinates for genes and transposable elements were obtained from UCSC genome browser. Density plot of signal enrichment was generated by bamCoverage, computeMatrix and plotHeatmap of the Python package deepTools (v3.5.1)[62]. ChIP-seq peak annotations were conducted using the R package ChIPseeker (v1.34.1)[63]. In order to facilitate the calculation process, the promoter region was defined as -2kb to +2 kb surrounding TSS (TSS ± 2 kb), and the gene body region was defined as +2 kb downstream of the TSS to TES of individual genes. The CpG density per 100 bp of the promoter region was calculated using the cpgDensityCal function of the R package Repitools (v1.36.0). K-means clustering for developmental stages was performed by R package ClusterGVis (v 0.0.2). Sankey

diagram was performed by R package ggalluvial (v0.12.4). Violin plot, heatmap, dot chart, box plot and bar plot were generated by ggplot2 in R (v3.4.3). The enrichment of TEs was calculated by the ratio of the length of TEs in peaks to the width of total peaks versus the ratio of the length of TEs to the chromosome size of the mouse genome. For the enrichment index of individual TE families, we first calculated normalized counts per TE transcripts by multiplying the density of individual TE transcript by its length, then we summarized counts of all TE transcripts belonging to the specific TE family, and finally we divided these counts by the total length of the specific TE family. To calculate distance between TSSs and adjacent distal SINE/B1 elements, all SINE/B1 elements were annotated in accordance with the GENCODE annotation (vM23), and only the most adjacent SINE/B1 elements of each gene were used for calculating the distances.

Low-input whole genome bisulfite sequencing (wgbs) of embryos and data analysis

A total of 8-10 early embryos were collected in each group. The WGBS libraries were prepared using a Post-bisulfite adapter tagging (PBAT) approach by Annoroad Gene Technology. Paired-end reads for each sample was generated by PE150 sequencing using Illumina HiSeq 3000 (Annoroad Gene Technology, China).

Raw reads were processed with Trim Galore (v0.6.4) to remove adaptor sequences and poor-quality bases with "-q 20 -phred33 -stringency 5 -length 20 -paired." Trimmed reads were then aligned to the mouse reference genome (mm10) using Bismark (v0.22.3) with the parameters "-p 6 -parallel 1 -N 0 -L 20 -quiet -pbat -un -un-ambiguous -bam." SAMtools (v1.3.1) was used to sort bam files by genomic coordination and make a bam file index. PCR duplicates were removed using Picard (v2.23.3). The methylation level at each CpG site was calculated using bismark_methylation_extractor model with the parameters "-p -comprehensive -no_overlap -bedgraph -counts -report -cytosine_report -gzip -buffer-size 30 G". The R package methylKit (v1.14.2)[64] was used to identify DMRs. The methylation levels at CpG sites were firstly calculated by "methRead" function with mincov = 3. Methylation across the genome was tiled with the 'tileMethylCounts' function using the parameters "win.size = 500, step. size = 500, cov. bases = 5", then 'unite' function was used to unite tiled regions with the "destrand = TRUE" parameter. At last, "calculateDiffMeth" function was used to calculate DMRs. DMRs with a minimum of 3 CpG sites and absolute methylation mean difference >25% and q-value < 0.05 were used for further analysis. The UCSC Genome Browser utility, bedGraphToBigWig, was used to transform the bedgraph files to bigwig files. UCSC genome browser was used for visualization.

Statistical analysis

GraphPad Prism 8.0 was used for calculations. Each experiment was repeated for at least three times, two-tailed unpaired Student's t-test or Mann-Whitney U test was used to calculate P values. Two-tailed Pearson correlation analysis was used to calculate r and P-values. Significance was determined by a P value < 0.05, ns was considered as not significant ($P > 0.05$). Scatterplots analysis of correlation was plotted with ggplot2 using Pearson correlation analysis.

Reporting summary

Further information on research design is available in the Nature Portfolio Reporting Summary linked to this article.

Data availability

The RNA-seq, ChIP-seq, and DNA methylome datasets of mouse oocyte and embryo in this study have been deposited to NCBI: GSE276707, GSE276706, and GSE276525. The ChIP-seq data of human embryo in this paper have been deposited in the Genome Sequence Archive in National Genomics Data Center, China National Center for Bioinformation/Beijing Institute of Genomics, Chinese Academy of Sciences (https://ngdc.cncb.ac.cn/gsa-human; GSA-Human: HRA008491). Previously published data used in this study are as follows: GSE241388, GSE169632, GSE169632, GSE215813, GSE36552. Source data are provided with this paper.

References

1. Wei, J. et al. Temporospatial hierarchy and allele-specific expression of zygotic genome activation revealed by distant interspecific urochordate hybrids. *Nat. Commun.* **15**, 2395 (2024).
2. Schulz, K. N. & Harrison, M. M. Mechanisms regulating zygotic genome activation. *Nat. Rev. Genet.* **20**, 221–234 (2019).
3. Wang, C. et al. Dynamic nucleosome organization after fertilization reveals regulatory factors for mouse zygotic genome activation. *Cell Res.* **32**, 801–813 (2022).
4. Zhang, B. et al. Widespread enhancer dememorization and promoter priming during parental-to-zygotic transition. *Mol. cell* **72**, 673–686.e676 (2018).
5. Li, J. et al. Metabolic control of histone acetylation for precise and timely regulation of minor ZGA in early mammalian embryos. *Cell Discov.* **8**, 96 (2022).
6. Feng, Y. et al. BRPF3-HBO1 regulates replication origin activation and histone H3K14 acetylation. *EMBO J.* **35**, 176–192 (2016).
7. Shi, L. H. et al. Trichostatin A (TSA) improves the development of rabbit-rabbit intraspecies cloned embryos, but not rabbit-human interspecies cloned embryos. *Developmental Dyn.: Off. Publ. Am. Assoc. Anatomists* **237**, 640–648 (2008).
8. Bu, G. et al. Coordination of zygotic genome activation entry and exit by H3K4me3 and H3K27me3 in porcine early embryos. *Genome Res.* **32**, 1487–1501 (2022).
9. Wu, K. et al. Dynamics of histone acetylation during human early embryogenesis. *Cell Discov.* **9**, 29 (2023).
10. Xu, R. et al. Stage-specific H3K9me3 occupancy ensures retrotransposon silencing in human pre-implantation embryos. *cell stem cell* **29**, 1051–1066.e1058 (2022).
11. Chen, Z., Djekidel, M. N. & Zhang, Y. Distinct dynamics and functions of H2AK119ub1 and H3K27me3 in mouse preimplantation embryos. *Nat. Genet.* **53**, 551–563 (2021).
12. Tan, M. et al. Identification of 67 histone marks and histone lysine crotonylation as a new type of histone modification. *Cell* **146**, 1016–1028 (2011).
13. Fang, Y. et al. Histone crotonylation promotes mesoendodermal commitment of human embryonic stem cells. *Cell Stem Cell* **28**, 748–763.e747 (2021).
14. Sabari, B. R. et al. Intracellular crotonyl-CoA stimulates transcription through p300-catalyzed histone crotonylation. *Mol. cell* **58**, 203–215 (2015).
15. Yuan, H. et al. Lysine catabolism reprograms tumour immunity through histone crotonylation. *Nature* **617**, 818–826 (2023).
16. Tang, X. et al. Short-Chain enoyl-CoA hydratase mediates histone crotonylation and contributes to cardiac homeostasis. *Circulation* **143**, 1066–1069 (2021).
17. Qu, Y. Y. et al. Inactivation of the AMPK-GATA3-ECHS1 pathway induces fatty acid synthesis that promotes clear cell renal cell carcinoma growth. *Cancer Res.* **80**, 319–333 (2020).
18. Hao, S. et al. Dynamic switching of crotonylation to ubiquitination of H2A at lysine 119 attenuates transcription-replication conflicts caused by replication stress. *Nucleic acids Res.* **50**, 9873–9892 (2022).
19. Liu, X. et al. MOF as an evolutionarily conserved histone crotonyltransferase and transcriptional activation by histone acetyltransferase-deficient and crotonyltransferase-competent CBP/p300. *Cell Discov.* **3**, 17016 (2017).
20. Seto, E. & Yoshida, M. Erasers of histone acetylation: the histone deacetylase enzymes. *Cold Spring Harb. Perspect. Biol.* **6**, a018713 (2014).

21. Jiang, G., Li, C., Lu, M., Lu, K. & Li, H. Protein lysine crotonylation: past, present, perspective. *Cell death Dis.* **12**, 703 (2021).
22. Liu, S. et al. Chromodomain Protein CDYL acts as a crotonyl-CoA hydratase to regulate histone crotonylation and spermatogenesis. *Mol. cell* **67**, 853–866.e855 (2017).
23. Zhou, C. et al. Global crotonylome identifies EP300-regulated ANXA2 crotonylation in cumulus cells as a regulator of oocyte maturation. *Int. J. Biol. macromolecules* **259**, 129149 (2024).
24. Fang, F. et al. Quantitative proteomics reveals the dynamic proteome landscape of zebrafish embryos during the maternal-to-zygotic transition. *iScience* **27**, 109944 (2024).
25. Chen C., et al. ENL reads histone β-hydroxybutyrylation to modulate gene transcription. *Nucleic Acids Res.* 10.1093/nar/gkae504 (2024).
26. Wang, J. et al. Acetate reprogrammes tumour metabolism and promotes PD-L1 expression and immune evasion by upregulating c-Myc. *Nat. Metab.* **6**, 914–932 (2024).
27. Zhang, Y. R. et al. Deciphering transcription activity of mammalian early embryos unveils on/off of zygotic genome activation by protein translation/degradation. *Cell Rep.* **44**, 115215 (2025).
28. Takahashi, S. et al. Embryonic genome instability upon DNA replication timing program emergence. *Nature* **633**, 686–694 (2024).
29. Wang, C. et al. Reprogramming of H3K9me3-dependent heterochromatin during mammalian embryo development. *Nat. cell Biol.* **20**, 620–631 (2018).
30. Abe, K. I. et al. Minor zygotic gene activation is essential for mouse preimplantation development. *Proc. Natl Acad. Sci. USA* **115**, E6780–e6788 (2018).
31. Shao, W. et al. Histone Methyltransferase SETD2 is required for porcine early embryonic development. *Animals: an open access journal from MDPI* **12**, (2022).
32. Ji, S. et al. OBOX regulates mouse zygotic genome activation and early development. *Nature* **620**, 1047–1053 (2023).
33. Skene, P. J. et al. Neuronal MeCP2 is expressed at near histone-octamer levels and globally alters the chromatin state. *Mol. cell* **37**, 457–468 (2010).
34. Lyst, M. J. et al. Rett syndrome mutations abolish the interaction of MeCP2 with the NCoR/SMRT co-repressor. *Nat. Neurosci.* **16**, 898–902 (2013).
35. Brooks K. E. et al. Molecular contribution to embryonic aneuploidy and karyotypic complexity in initial cleavage divisions of mammalian development. *Development (Cambridge, England)* **149**, (2022).
36. Hamatani, T., Carter, M. G., Sharov, A. A. & Ko, M. S. Dynamics of global gene expression changes during mouse preimplantation development. *Developmental cell* **6**, 117–131 (2004).
37. Wu, Y. et al. N(6)-methyladenosine regulates maternal RNA maintenance in oocytes and timely RNA decay during mouse maternal-to-zygotic transition. *Nat. cell Biol.* **24**, 917–927 (2022).
38. Xu, G. & Law, J. A. Loops, crosstalk, and compartmentalization: it takes many layers to regulate DNA methylation. *Curr. Opin. Genet. Dev.* **84**, 102147 (2024).
39. Xie, S. Q. et al. Nucleolar-based Dux repression is essential for embryonic two-cell stage exit. *Genes Dev.* **36**, 331–347 (2022).
40. Gao, D. et al. P300 regulates histone crotonylation and preimplantation embryo development. *Nat. Commun.* **15**, 6418 (2024).
41. Li, Y. et al. Molecular Coupling of Histone Crotonylation and Active Transcription by AF9 YEATS Domain. *Mol. cell* **62**, 181–193 (2016).
42. Kang, M. H., You, S. Y., Hong, K. & Kim, J. H. DMSO impairs the transcriptional program for maternal-to-embryonic transition by altering histone acetylation. *Biomaterials* **230**, 119604 (2020).
43. Riesle, A. J. et al. Activator-blocker model of transcriptional regulation by pioneer-like factors. *Nat. Commun.* **14**, 5677 (2023).
44. Yan, Y. L. et al. DPPA2/4 and SUMO E3 ligase PIAS4 opposingly regulate zygotic transcriptional program. *PLoS Biol.* **17**, e3000324 (2019).
45. Li, S. et al. Capturing totipotency in human cells through spliceosomal repression. *Cell* **187**, 3284–3302.e3223 (2024).
46. Burgin, H. et al. Loss of mitochondrial fatty acid β-oxidation protein short-chain Enoyl-CoA hydratase disrupts oxidative phosphorylation protein complex stability and function. *FEBS J.* **290**, 225–246 (2023).
47. Nagaraj, R. et al. Nuclear localization of mitochondrial TCA cycle enzymes as a critical step in mammalian zygotic genome activation. *Cell* **168**, 210–223.e211 (2017).
48. Lee, M. T., Bonneau, A. R. & Giraldez, A. J. Zygotic genome activation during the maternal-to-zygotic transition. *Annu. Rev. cell developmental Biol.* **30**, 581–613 (2014).
49. Tian, Q. et al. Chromatin Modifier EP400 regulates oocyte quality and zygotic genome activation in mice. *Adv. Sci. (Weinh.)* **11**, e2308018 (2024).
50. Pal, M., Altamirano-Pacheco, L., Schauer, T. & Torres-Padilla, M. E. Reorganization of lamina-associated domains in early mouse embryos is regulated by RNA polymerase II activity. *Genes Dev.* **37**, 901–912 (2023).
51. Liu, B. et al. The landscape of RNA Pol II binding reveals a stepwise transition during ZGA. *Nature* **587**, 139–144 (2020).
52. Wang, M., Chen, Z. & Zhang, Y. CBP/p300 and HDAC activities regulate H3K27 acetylation dynamics and zygotic genome activation in mouse preimplantation embryos. *EMBO J.* **41**, e112012 (2022).
53. Yu, H. et al. Global crotonylome reveals CDYL-regulated RPA1 crotonylation in homologous recombination-mediated DNA repair. *Sci. Adv.* **6**, eaay4697 (2020).
54. Guo, Z. et al. Hypoxia-induced downregulation of PGK1 crotonylation promotes tumorigenesis by coordinating glycolysis and the TCA cycle. *Nat. Commun.* **15**, 6915 (2024).
55. Gassler, J. et al. Zygotic genome activation by the totipotency pioneer factor Nr5a2. *Sci. (N. Y., NY)* **378**, 1305–1315 (2022).
56. Ohnishi, Y. et al. Active role of small non-coding RNAs derived from SINE/B1 retrotransposon during early mouse development. *Mol. Biol. Rep.* **39**, 903–909 (2012).
57. Fu, H. et al. Dynamics of telomere rejuvenation during chemical induction to pluripotent stem cells. *Stem cell Rep.* **11**, 70–87 (2018).
58. Sherman, B. T. et al. DAVID: a web server for functional enrichment analysis and functional annotation of gene lists (2021 update). *Nucleic Acids Res* **50**, W216–W221 (2022).
59. Huang da, W., Sherman, B. T. & Lempicki, R. A. Systematic and integrative analysis of large gene lists using DAVID bioinformatics resources. *Nat. Protoc.* **4**, 44–57 (2009).
60. Zhang, Y. et al. Model-based analysis of ChIP-Seq (MACS). *Genome Biol.* **9**, R137 (2008).
61. Kuhn, R. M., Haussler, D. & Kent, W. J. The UCSC genome browser and associated tools. *Brief. Bioinform* **14**, 144–161 (2013).
62. Ramirez, F. et al. deepTools2: a next generation web server for deep-sequencing data analysis. *Nucleic Acids Res* **44**, W160–W165 (2016).
63. Yu, G., Wang, L. G. & He, Q. Y. ChIPseeker: an R/Bioconductor package for ChIP peak annotation, comparison and visualization. *Bioinformatics* **31**, 2382–2383 (2015).
64. Akalin, A. et al. methylKit: a comprehensive R package for the analysis of genome-wide DNA methylation profiles. *Genome Biol.* **13**, R87 (2012).

Acknowledgements

This work was supported by the National Natural Science Foundation of China (32470858 to LQ.Z., 82471669 to QZ.X., 82401956 to Q.T.), Shanghai Key Laboratory of Reproduction and Development (Redlab202404 to LQ.Z.), Fertility Research Program of Young and Middle-aged Physicians in 2024 (BJHPA-2024-SHZHYXZHQNYJ-006 to QR.Q.), the Key Research Program of Hubei Province of China (2021BCA107 to QZ.X.), and the Program for HUST Academic Frontier Youth Team (to

LQ.Z.). We thank all the lab members of LQ.Z. for the helpful discussion of the manuscript. The authors also thank the Laboratory Animal Center, Huazhong University of Science and Technology, for providing technical support on mouse breeding.

Author contributions

Y-F.W., Y-T.W. and Q-R.Q. contributed equally to this work. Y-F.W. and Y-T.W. performed the animal experiments and data analysis, and wrote the initial manuscript. Y-T. W. completed the task of illustrating the picture. Y-F.W. and Q-R.Q. collected the human embryos for examination and helped with the immunostaining experiments. Q.T. helped with embryo collection and CUT&Tag assay. X-M.L. helped with the experimental design and provided valuable guidance. L-Q.Z., Y.Y. and Q-Z.X. conceived, designed, and supervised the study. Y.Y. performed high-throughput data analysis. Q-Z.X. improved pharmacological treatment study. L-Q.Z. and Y.Y. revised the manuscript. All authors contributed to the article and approved the manuscript.

Competing interests

The authors declare no competing interests.

Additional information

Supplementary information The online version contains supplementary material available at https://doi.org/10.1038/s41467-025-60565-z.

Correspondence and requests for materials should be addressed to Qing-zhen Xie, Ying Yin or Li-quan Zhou.

Peer review information *Nature Communications* thanks the anonymous, reviewer(s) for their contribution to the peer review of this work. A peer review file is available.